Paleo-environment and provenance in a lacustrineshallow-water delta - meandering river sedimentary system: Insights from the Middle-Upper Jurassic formations of the Fukang Sag of Junggar Basin, NW China.

Long Luo[a,b,c], Xianzhi Gao[a,b]*, Xianfeng Tan[d], Jon Gluyas[c], Jinduo Wang[e], Xiangye Kong[f], Jinzhao Huang[g], Hengbo Shao[a] , Futao Qu[a]

[a] College of Geosciences, China University of Petroleum, Beijing 102249, China

[b] State Key Laboratory of Petroleum Resources and Prospecting (China University of Petroleum, Beijing), Beijing102249, China

[c] Department of Earth Sciences, Durham University, Durham, DH1 3LE, UK

[d] Chongqing Key Laboratory of Complex Oil and Gas Field Exploration and Development, Chongqing University of Science and Technology, Chongqing 401331, China.

[e] Exploration and Development research institution, Shengli Oilfield Branch Company of Sinopec

[f] Unconventional Natural Gas Institute, China University of Petroleum, Beijing, 102249, China

[g] Second oil production plant of Changqing Oilfield Company, China National Petroleum Corporation, Qingyang 744100, China.

*Corresponding authors: College of Geosciences, China University of Petroleum (Beijing), 18 Fuxue Road, Changping District, Beijing 102249, China.

*E-mail addresses: gaoxz1963@163.com (X. Gao), longluo988@163.com (L. Luo),

Abstract

The Middle-Upper Jurassic Shishugou Group in the central Junggar Basin was deposited in a lacustrine -shallow water delta-meandering river sedimentary system. The integrated petrological (thin-section, granularity and heavy minerals analysis), geochemical (trace elements and rare earth elements analysis) and geophysical analyses (well logging and 3D-seismic slice analysis) are intended to revealthe redox conditions, palaeo-climate, palaeo-salinity, provenance and sedimentary evolution extant during deposition of the Shishugou Group and determine the relationships among them: the redox condition changed from a weak anoxic/oxic condition to a strongly oxic condition; the climate changed from humid to hot and arid in the Middle-Late Jurassic, which may have resulted in the lake water having slight – medium salinity; the relatively distant northeastern provenance from Kelameili Mountain is the most important sediment source, and the south provenance from the Tianshan Mountains (Bogeda Shan) decreases with the development of the Sag piedmont, which only supplies sediments for the southeastern Fukang Sag. The sedimentary environment changed from a lake - shallow water delta to a meandering river during the deposition of the Shishugou Group. The shallow-water meandering river delta was characterized by pervasive mudstones with oxide colours, thin single-layer sand bodies (1-15 m, av.3m), relatively low sand-strata ratios (0.2-0.5) and the lack of progradation, mouth bar and reverse rhythm.The gentle slope is the primary condition necessary for the formation of a shallow-water meandering river delta. Palaeo-environment (climate change from Warm-humid to hot-arid) and stable and far Kelameili Mountain provenance played critical roles in the development and evolution of lacustrine- delta-meandering river sedimentary systems.

Keywords

Palaeoclimate; Redox condition; Palaeosalinity; Warm humid; Hot arid; Shishugou Group; Fukang Sag

1. Introduction

The provenance, palaeo-environment including palaeoclimate, redox conditions and palaeo-salinity are important factors used to decipher the sedimentary distribution and evolution and are key in revealing the relationship among the palaeo-environment, provenance and evolution of the depositional system (Lv et al., 2016; Potter-Mclntyre et al., 2016, Lv et al., 2017). The climate, which may determine the lake level, redox condition and salinity, is one of most important environmental controls on sedimentary characteristics (Engelmann et al., 2004; Jone et al., 2014; Lv et al., 2014; Kim et al., 2015; Lv et al., 2017; Liu et al., 2018). The concept of shallow-water delta was proposed in 1954 (Fisk et al.,1954). The lacustrine shallow-water delta is generally formed in comprehensive conditions including shallow water depth (less than several tens of meters), gentle slope, lake level change and stable provenance.Besides, it is characterized by hot-arid climate, pervasive red mudstone, fine-grained sandstone, thin single sand-body and low ratio of sandstone in strata (Lemons and Chen,1999; Zhu et al.,2012; Zhu et a.,2013; Zhu et al.,2016).

The Jurassic was a typical greenhouse period and was predominantly characterized by global warmth and atmospheric CO_2 levels as much as four times as large as the present (Berner and Geocarb, 1994; Huber et al., 2000; Sellwood and Valdes, 2008). Hence, the Jurassic palaeoclimate has been one of the popular topics of sedimentary environment research (Moore et al., 1992; Berner and Geocarb, 1994; Huber et al., 2000; Sellwood and Valdes, 2008; Myers et al., 2011; Galloway et al., 2013; Wierzbowski et al., 2013; Souto and Fernandes, 2017; El-Sabbagh et al., 2017; Martínez-Yanez et al., 2017). There were five stages of palaeoclimatic evolution in China, and the palaeoclimate regionalization was different during these stages (Deng et al., 2017). The Jurassic formations of the Junggar Basin of northwestern China are currently important hydrocarbon exploration targets, especially the Fukang Sag, which is located in the centre of the Junggar Basin. Moreover, the sedimentary characteristics of Middle-Upper Jurassic formations have remarkable variability, perhaps due to the palaeoclimate conditions and provenance. However, few publications referencing the Jurassic palaeoclimate of the Junggar Basin of China exist (Deng et al., 2017; Zhu et al., 2017).

The provenance of the Jurassic Shishugou Group is almost universally accepted in the eastern Fukang slope of central Junggar basin, but thereis some controversy in the central and eastern Fukang Sag (e.g. the fourth region of Central Junggar basin) (Zhang et al.,1999;Shang et al.,2011; Ji et al.,2014;Su et al.,2014).

The primary objective of this study is to determine the provenance of the clastic rock and the palaeoenvironmental conditions present during the Middle-late Jurassic period in the Junggar Basin. This study also aims to reveal the relationship between the palaeo-environment, provenance and lake-shallow water delta- meandering river sedimentary system.

2. Geological setting

The Junggar Basin is located in Xinjiang Uygur Autonomous Region , northwestern China. The subtriangular basin is surrounded by six mountains formed by belts of thrust faults (Fig. 1). The northwestern boundary is defined by Zaire Mountain and Halahaalate Mountain; the northeastern boundary is defined by Qinggelidi Mountain and Kelameili Mountain; and the southern boundary is defined by the North Tianshan, including Eren Habirga Mountain and Bogeda Mountain (Fig. 1)（Luo et al.,2018; Wang et al.,2018）. The Fukang Sag, which is located close to the central Junggar Basin, is a piedmont Sag of North Tianshan (Fig. 1).

The initial uplift of the southern part of Bogeda Mountain occurred in the early-middle Jurassic（Greene, 2001； Gong et al., 2015）. The rapid uplift of both southern Bogda Mountain and northeastern Kelameili Mountain occurred in the early Jurassic but slowed in the middle Jurassic. The uplift of Bogda Mountain was clearly faster than that of northeastern Kelameili Mountain during the deposition of the Shishugou Group (Gong et al., 2015）. Consequently, the Fukang Sag now slopes gently to the southwest (Luo et al., 2018).

The formations that comprise the Jurassic stratum include the Badaowan (J_1b), Sangonghe (J_1s), Xishanyao (J_2x), Toutunhe (J_2t) and Qigu (J_3q) Formations (Fig. 2). The regional angular unconformity on the top of the Qigu Formation (Fig. 2) was formed by the tectonic uplift of the Junggar Basin (Wu, 1986; Li et al., 2006). Qigu Formation has been strongly eroded because of the unconformity, so the remaining Qigu Formation is thin and difficult to be identified accurately. Moreover, both Toutunhe and Qigu Formation are very important to the research of paleo-environment and sedimentary evolution. Therefore, we usually research them together as the Shishugou Group. The Middle-late Jurassic Shishugou Group comprising Toutunhe and Qigu Formations were buried to a depth of 3600-5800 m, deposited in a lacustrine-deltaic-meandering fluvial sedimentary system in the Fukang Sag (Zhu et al., 2017). The Toutunhe Formation consists of the first member (J_2t^1), the second member (J_2t^2) and the third member (J_2t^3). The lacustrine basin depth clearly decreased during the deposition of the Shishugou Group, meanwhile, the palaeoclimate became clearly hot and dry (Fig. 2) (Zhu et al., 2017).

According to high-resolution sequence stratigraphy (Cross, 1994), the Shishugou Group in the Junggar Basin exhibits two long-term stratigraphic base-level circles (3rd-order sequences), as shown in Fig. 2. The Toutunhe Formation can be divided into one long-term stratigraphic base-level cycle (LSC), and subdivided into three middle base-level cycles (MSC1, MSC2, MSC3) and ten short cycles (SSC1-SSC10) (Fig. 2). The Qigu Formation, which consists of one LSC, can be divided into three middle base-level cycles (MSC1, MSC2, MSC3) and subdivided into at most eight short cycles (SSC1-SSC8) (Fig. 2) (Zhang et al., 2000; Wang et al., 2001; Yu et al., 2014; Yu et al., 2016). The Qigu Formation is generally composed of less than eight SSC due to the erosion represented by the upper unconformity (Fig. 2).

3. Materials and methods

Datasets used in this investigation consist of seismic slices, well logs, conventional cores and outcrop sections. The three-dimensional seismic data consists of three parts and covers most of the Fukang Sag. The seismic slices with amplitude attributes are chopped nearly along the layer or target formation. Fifty-six representative core samples were collected from the Toutunhe and Qigu Formations, from 8 wells and 10 outcrop samples from the field section in the Fukang Sag. Thirty-two thin sections, which were impregnated with blue epoxy resin, were used for petrological and mineralogical analyses by 300-point counts. The granularity analysis was performed on 28 sandstone samples by measuring 400 grains per thin section under a microscope.

The original geochemical signatures of mudstone can remain relatively well-preserved during deposition due to its grain size and impermeability (McCulloch and Wasserburg, 1978; Sochava et al., 1994; Cullers, 1995; Graver and Scott, 1995). The current geochemical characteristics of a mudstone include trace elements and rare earth elements, which are deposited in sedimentary basins without significant fractionation, generally preserving the original signature of the source materials (Floyd et al., 1990). Therefore, the current geochemical characteristics of mudstones are widely used in provenance studies of clastic rocks (Dickinson and Suczek, 1979; Bhatia, 1983; McLennan et al., 1983; Bhatia and Crook, 1986; Roser and Korsch, 1986; McLennan and Taylor, 1991; Owen et al., 1999;). In addition, some trace elements (e.g., Sr, Cu, and Rb) in the mudstone, which are sensitive to palaeoenvironmental parameters, are generally used to decipher the palaeotectonic setting and the palaeoclimate conditions (Worash, 2002; Zhang et al., 2006; Zhao et al., 2007; Cao et al., 2012). Eleven mudstone samples were collected from cores of the 7 wells; 6 of the samples come from the J_3q, and 5 come from the J_2t. The trace elements and Rare Earth Elements (REE) of 11 mudstone samples were analysed using ICP-MS (DRC-e). Repeated analysis of USGS reference materials OU-6, AMH-1 and GBPG-1 shows that the analytical precision of most trace elements was better than 95%.

In addition, most heavy minerals are derived from specific source rocks and controlled by their provenance; therefore, heavy mineral analysis is the most common techniques for provenance determination (Morton and Hallsworth, 1999; Svendsen and Hartley, 2002; Mange and Wright, 2007; Garzanti et al., 2008; Morton et al., 2011; Nieet al., 2012; Sevastjanova et al., 2012; Do Nascimento Jr et al., 2015; Bassis et al., 2016; Aubrecht et al., 2017). The heavy mineral composition of a source rock can be altered and modified by many processes such as chemical weathering, hydraulic sorting during transport, sorting by grain size, diagenetic alteration during deposition and burial processes (Morton and Hallsworth, 1999; Garzanti et al.,2008, 2009). Therefore, some heavy mineral (HM) assemblages, which are sensitive to their environment, can also be used to evaluate the approximate palaeogeographic conditions, including palaeoclimate, palaeo-environment and palaeotopography (Parfenoff et al., 1970; Mange and Maurer, 1992; Dill, 1998; Jin et al., 2002; Dinis and Soares, 2007; Lin et al., 2008; Liu, 2012). Heavy minerals analysis was performed on 30 samples, which were collected from the Toutunhe and Qigu Formations, to identify the species, characteristics and contents of the heavy minerals. Moreover, the heavy mineral data of 56 samples in East Fukang slope were collected from Xinjiang Oil field and previous published results (Ji et al.,2014).

4. Results

4.1 Petrology of sandstones

The Shishugou Group sandstones in the Fukang Sag are predominantly litharenite, according to Folk's (1980) sandstone classification scheme, averaged as $Q_{43.8}F_{7.4}R_{48.8}$

(Luo et al. 2018). Lithic grains (R) are the most common detrital component, representing approximately 48.8% (average value) of the detrital grain volume and consisting of volcanic, metamorphic and minor sedimentary rock fragments (Fig. 3a-f) (Luo et al., 2018). The detrital grains, which are characterized by poor to moderate sorting, are mostly fine-grained but also contain a small number of silty and medium-sized grains (Fig. 3). The rock fragments of the J_2t conglomerate sampled from outcrop consist of volcanic and metamorphic rock fragments (Fig. 3g-i). The rock fragments of the J_3q medium sandstone from outcrop mostly comprise metamorphic rock fragments, with a minor constituent of volcanic rock fragments (Fig. 3g-i).

4.2 Heavy minerals of sandstone

The heavy mineral assemblages mainly comprise epidote (relative content: 0% to 84.7%, av. 32.4%), limonite (relative content: 0%-81.7%; av. 23.8%), garnet (relative content: 0%-25.9%, av. 4.6%), zircon (relative content: 0%-21.1%, av. 3.5%), barite (relative content: 0%-76.9%, av. 12.1%), magnetite (0%-16.9%, av. 3.2%) and pyrite (relative content: 0%-99.1%, av. 8.3%) (Table 1). Pyrite occasionally occurs at the strata of certain wells, such as the D1, D7 and D11 wells, and is mainly observed in the first (J_2t^1) and second (J_2t^2) sub-member of the Toutunhe Formation sandstones (Table 1, Fig. 4, Fig. 5). The abundance of limonite increases as the age of the sandstones decreases (Fig. 6, Fig. 7). The relative limonite content of the first sub-member of the Toutunhe Formation (J_2t^1) sandstones ranges from 0.0% to 1.8% (av. 0.3%); the limonite content of the second sub-member (J_2t^2) sandstones varies from 0.0% to 81.7% (av. 29.3%); the limonite content of the third sub-member (J_2t^3) sandstones varies from 0.2% to 61.2% (av. 31.1%); and the limonite content of the Qigu Formation (J_3q) sandstones varies from 20.2% to 67% (av. 50.5%)(Table 1).

The ZTR values of Shishugou Group sandstones vary from 0.1 to 66.4 (with an average value of 9.7). The Qigu Formation (J_3q) sandstones have ZTR values ranging from 1.7 to 16.5 (av. 7.0) (Table 1). The ZTR values of the Toutunhe Formation sandstones varies from 0.1 to 66.4 (with an average value of 10.0); the first sub-member of Toutunhe Formation (J_2t^1) sandstones have ZTR values ranging from 0.1 to 66.4 (av. 17.2); the ZTR values of the second sub-member (J_2t^2) sandstones vary from 0.4 to 28.5 (with an average value of 8.0); and the ZTR values of the third sub-member (J_2t^3) sandstones vary from 0.2 to 9.9 (with an average value of 3.2) (Table 1).

4.3 Trace element geochemistry of mudstone

The abundance of 33 trace elements in the mudstones has been measured to reconstruct the palaeoenvironment. Representative ratios (Rb/Sr, Sr/Cu, Sr/Ba, U/Th and V/Cr) can help to unravel the palaeoenvironment (palaeoclimate, palaeosalinity and redox conditions) (Epstein and Mayeda, 1953; Lerman and Gat, 1989; Zheng and Liu., 1999; Jin and Zhang, 2002; Meng et al., 2012; Bai et al., 2015; Moradi et al., 2016; Cao et al., 2015; Moradi et al., 2016). The Sr/Ba ratio varies from 0.34 to 0.62 with an average value of 0.48. The U/Th ratio varies from 0.10 to 0.48 with an average value of 0.26. The Sr/Cu ratio varies from 1.38 to 16.19 with an average value of 6.82. The V/Cr ratio varies from 0.43 to 2.59 with an average value of 1.30 (Table 2). The vertical profiles of the redox-sensitive elements measured (Cd, U, Ta and Mo) and their related ratios (Rb/Sr, Sr/Cu, Sr/Ba, U/Th and V/Cr) in the mudstones are illustrated in Fig. 8. Raw data are provided in Table 2.

4.4 REE geochemistry of mudstone

The total Rare Earth Element (REE) concentrations in the Shishugou Group mudstone varies from 146.47 ppm to 1413.04 ppm (with an average value of 442.61 ppm) (Table 3). The shale-normalised (NASC) REE concentration is characterized by an essentially flat pattern, with La_N /Yb_N values varying from 0.8 to 1.35 (av. 1.06)

(Table 3, Fig. 9). In addition, they have a relative enrichment of light REE (LREE), with Ce_N /Yb_N values ranging from 0.94 to 16.97 (av. 4.79) (Table 3, Fig. 9). The REE concentrations of three samples (D8-6, D3-7, D6-6) markedly peak at Ce, with an additional peak at Er (Table 3, Fig. 9).

Most REE, especially Ce, Er and Gd, have relatively high concentrations in the middle-upper part of J_2t^2 and the middle-lower part of the J_2t^3 and relatively low concentrations in the other parts of the Shishugou Group (Fig. 10). The microfacies of all samples from J_2t^2 and D6-6 from J_3q mainly include subaqueous interdistributary bay and subaqueous natural levee.

The relative enrichment or depletion in Ce relative to La and Pr is expressed as the Ce anomaly and is quantified as the ratio $Ce/Ce^* = (Ce_N)/(La_N + Pr_N) \times 0.5$, where N represents the shale-normalized (NASC) values (Murray et al. 1992). The Eu anomaly was calculated by $Eu/Eu^* = Eu_N/(Sm_N + Gd_N) \times 0.5$ (Murray et al., 1992; Owen et al., 1999). The Ce/Ce* values are almost all less than 1, representing a negative anomaly, but three samples (such as D8-6, D3-7, and D6-6) are greater than 1, representing a positive anomaly (Table 3). The Eu/Eu* values of all samples are less than 1, which represents a negative anomaly. La_N /Yb_N values vary from 0.8 to 1.35 with an average value of 1.06 (Table 3).

4.5 Sedimentary facies

4.5.1 Facies association A (Shore-shallow lacustrine facies)

4.5.1.1 Description

The lithofacies of facies association A is composed of grey-dark grey mudstone, siltstone and fine sandstone (Fig. 11). The lithofacies associations were characterized by sandstone/mudstone couplets that form a rhythmically interbedded succession at several metres to ten metres in scale (Fig. 11). The sedimentary structures included wave ripples, current bedding, lenticular bedding, and cross bedding. Carbon fragments were distributed along the bedding plane (Fig. 11). In the cumulative curve of particle size, the probability of bar and beach sandstone consist of three sections, in which the bouncing-dominated component consists of two sections (Fig. 11). The well log gamma (GR) curve shows finger-, serrated- and funnel-shaped low amplitude variations (Fig. 11).

4.5.1.2 Interpretation

The carbon fragments may originate from the semi-deep to deep lacustrine environments. The grey-dark grey mudstones, siltstones and fine sandstones containing carbon fragments were deposited in a relatively deep-water environment near a semi-deep lacustrine environment. Furthermore, the interbedded relationship of the mudstone and sandstone, the well-log curve (GR), the cumulative particle size probability curve and the sedimentary structures present suggest that the shore-shallow lacustrine facies and the beach and bar sandstones are the most important sand bodies (Fig. 11). The facies association A can be interpreted as the shore-shallow lacustrine facies (Fig. 11).

4.5.2 Facies association B (Shallow-water meandering-river delta front)

4.5.2.1 Description

Lithofacies of facies association B include green grey-grey siltstone, fine sandstone (several metres to tens of metres in scale) and mudstone with a relatively low sand-strata ratio (0.2 to 0.5) (Fig. 12). The sedimentary structures include parallel bedding, current bedding, cross-bedding and basal erosion scouring structures, wave ripples, sphenoid cross-bedding, lenticular bedding and slump structures. The cumulative particle size probability curve of the main sand body, which has a relatively steep slope, comprise two sections representing the more abundant bouncing component and the more minor suspension-transport component (Fig. 12). The GR curve of the main sand body generally shows bell-shaped or box- and funnel-shaped middle amplitude variations. The GR curve of the interbedded siltstones and mudstones shows serrated low-amplitude variations (Fig. 12).

4.5.2.2 Interpretation

The main green grey- grey sand body exhibiting parallel bedding, current bedding, and cross-bedding was deposited in a shallow water environment and influenced by wave action. The basal erosional scour structures observed also suggest that the river channel was eroded. The slump structures and the cumulative particle size probability curve are generally indicative of a delta front environment (Fig. 12). Therefore, the main green grey-grey sand body can be interpreted as a subaqueous distributary channel of the delta front. The sand body with the funnel-shaped GR curve is likely a mouth bar, on the basis of characteristics of the cumulative curve (Fig. 12). The interbedded siltstone and mudstone succession may be interpreted as the subaqueous natural barrier of the delta front. The green grey-grey succession generally represents an interdistributary bay. Consequently, the facies association B represent a shallow-water meandering-river delta front (Fig. 12).

4.5.3 Facies association C (Shallow-water meandering-river delta plain)

4.5.3.1 Description

Lithofacies of facies association C comprise the grey-green, brown and brownish-red interbedded fine-sandstones and mudstones (Fig. 13). The sand-mud ratio (0.4-0.8) of the interbedded succession is lower than that of facies association B (0.8-1.2). The sedimentary structures observed include parallel bedding, current bedding, low-angle tabular/wedge-shaped cross-bedding and basal erosional scour structures. The cumulative particle size probability curve of the main sand body that has a relatively steep slope comprise three sections, representing the dominant bouncing transport and minor rolling and suspension transport (Fig. 13). The GR curve of the main sand body generally exhibits box-shaped middle-high amplitude variations and a bell-shape if the thickness of the sand body is relatively small. The GR curve of grey-green, brown and brownish-red interbedded siltstone and mudstone shows serrated low-amplitude variations (Fig. 13).

4.5.3.2 Interpretation

The grey-green, brown and brownish-red interbedded fine sandstone and mudstone unit that has a relatively low sand-mud ratio (0.4-0.8) is suggestive of an intermittently exposed shallow water environment. The grey-green and brown fine-sandstones with low-angle tabular/wedge-shaped cross-bedding and basal erosional scour structures indicate river channel erosion. In addition, the GR curve and the cumulative particle size probability curve of the main sand body also provide evidence for a channel branch of the delta plain (Fig. 13). Therefore, the grey-green, brown and brownish-red interbedded siltstones and mudstones can be interpreted as the natural barrier of the delta plain. The massive succession of grey-green, brown and brownish-red mudstone can be interpreted as an arid interchannel depression, which is different from a marsh (Fig. 13). Hence, facies association C should be interpreted as the shallow-water delta plain of a meandering river (Fig. 13).

4.5.4 Facies association D (Meandering river)

4.5.4.1 Description

Lithofacies of facies association D exhibit relatively low sand-mud ratios (0.2 to 0.5) and consist of brownish-red/taupe fine-medium sandstone, mudstone and some coarse sandstone (Fig. 14). The sedimentary structures observed include parallel bedding, low-angle tabular/wedge-shaped cross-bedding, and basal erosional scour structures. The climbing-ripple bedding and current bedding can be observed in the interbedded siltstone and mudstone succession. Horizontal bedding and lenticular bedding were observed in the mudstone succession. The cumulative particle size probability curve of the main sand body that has a relatively gentle slope comprise two sections representing bouncing and suspension transport; the relatively high percentages of suspension transport vary from 20% to 50% (Fig. 14). Some coarse sandstones consist of rolling, bouncing and suspension-transport components. The well-log gamma (GR) curve of the main sand body generally shows a dentate-box or dentate-bell shape and middle-high amplitude variations (Fig. 14). The GR curve of the brownish-red/taupe interbedded siltstone and mudstone shows serrated middle-low amplitude variations (Fig. 14).

4.5.4.2 Interpretation

The brownish-red/taupe lithofacies is indicative of an exposed oxidizing environment. The main fine-medium sand body has a relatively low sand-mud ratio and is characterized by low-angle tabular/wedge-shaped cross-bedding and basal erosional scour structures, suggestive of river channel erosion. In addition, the GR curve and the cumulative particle size probability curve also suggest that the main fine-medium sand body can be interpreted as a point bar and some of the coarse sandstone can be interpreted as a channel-lag deposit. The brownish-red/taupe interbedded siltstone and mudstone with climbing ripple bedding can be interpreted as a natural barrier. The brownish-red/taupe mudstone succession represents a floodplain. As a whole, facies association D was deposited in a meandering river environment (Fig. 14).

5. Discussions

5.1 Redox condition

The redox-sensitive parameters related to the geochemistry are widely used to qualitatively decipher palaeo-environment, palaeo-water depth and offshore distance because deep lacustrine settings are generally anoxic and shallow lacustrine to fluvial settings are mainly dysoxic to oxic (Algeo et al., 2010; Tan et al., 2017). The concentration and ratio value of redox-sensitive trace elements and rare earth elements are redox indicators of the palaeo-environment (Fig. 14) (Elderfield and Greaves, 1982; Barwise, 1990; Jones and Manning, 1994; Betchtal et al., 2001; Adegoke et al., 2014; Hu et al., 2016; Tan et al., 2017; Kuzyk et al., 2017).

The varying Ce^{3+} ion concentrations and redox condition are well demonstrated by the Ce anomaly in both marine and lacustrine settings, so the critical parameters (e.g., Ce_{anom}) related to the Ce anomaly are widely used to estimate the palaeo-redox conditions (Wilde et al., 1996). A positive cerium anomaly of the samples, characterized by Ce/Ce* values greater than 1, suggests low-oxygen depositional conditions. Conversely, a negative cerium anomaly, characterized by Ce/Ce* values less than 1, represents an oxidizing depositional environment (Murthy et al., 2004).

Most of the samples with negative cerium anomalies have Ce/Ce* values suggestive of oxidizing conditions, but three samples (D8-6, D3-7, D6-6) with positive anomalies are indicative of low-oxygen/reducing conditions (Table 3) (Murthy et al., 2004). A negative Eu/Eu* (less than 1) may indicate the preferential loss of Ca-bearing minerals during weathering and deposition or may reflect the sediment sources (Murthy et al. 2004). The negative anomaly of Eu/Eu* values in the Shishugou Group mudstone suggests oxidizing conditions (Table 3) (Sverjensky, 1984; Murthy et al., 2004).

The Th/U ratio was generally used to examine the redox conditions of the depositional environment (Wignall and Twitchett, 1996). U is mobile under oxic conditions but relatively immobile under anoxic conditions so anoxic sediments are much more enriched in U than oxic sediments (Baioumy and Lehmann, 2017). Th is stable under redox conditions and immobile in any aqueous environment. Therefore, low Th/U ratios or high U/Th ratios indicate reducing conditions. The ratio of U/Th, which ranges from 0.1 to 0.48 with an average value of 0.24, suggests that the Shishugou Group mudstones were mainly deposited in oxidizing conditions (Table 3, Fig. 8i) (Pi et al. 2014). The V/Cr ratios below 2 represent oxic depositional conditions; V/Cr ratios ranging from 2 to 4.25 suggest dysoxic conditions; and V/Cr ratios over 4.25 indicate an anoxic-suboxic environment (Jones and Manning, 1994). V/Cr values of the Shishugou Group range from 0.43 to 2.59, with an average of 1.30, and suggest that the Shishugou Group was mainly deposited in oxidizing conditions (Table 2, Fig. 8f).

The V/Ni ratio has been widely used to determine the redox condition present during deposition. V/Ni ratios higher than 3 indicate that mudstones were deposited under anoxic conditions, while V/Ni ratios varying between 1.9 and 3 indicate that mudstones were deposited in a dysoxic-oxic environment (Galarraga et al., 2008). The V/Ni ratios in the Shishugou Group mudstones, which vary between 0.81 and 3.38, with an average of 2.4, decrease as the age of the strata decreases (Table 2, Fig. 8k). Some mudstones of J_2t^1 and J_2t^2 have relatively high V/Ni ratios, higher than 3 (Table 2, Fig. 8k). These results indicate that the Shishugou Group mudstones were mainly deposited in a dysoxic-oxic environment and some mudstones of J_2t^1 and J_2t^2 may have been deposited in reducing conditions (Fig. 15, Fig. 16). Most of the Shishugou Group mudstones display V/(V + Ni) ratios below 0.8 and V/(V + Cr) ratios below 0.6, indicating the dysoxic-oxic condition present during their deposition (Tables 2, Fig. 9l-m, Fig. 15,Fig. 16) (Zhou and Jiang, 2009; Pi et al., 2014; Baioumy and Lehmann, 2017).

The occurrence of the heavy mineral pyrite generally reflects anoxic/reducing conditions or a warm humid climate present during deposition, and limonite suggests the presence of oxidizing conditions or a hot arid climate (Jin et al., 2002; Lin et al., 2008; Liu, 2012). Pyrite, which is mainly observed in the first (J_2t^1) and second (J_2t^2) sub-members of the Toutunhe Formation sandstones in some wells (Table 1, Fig. 4, Fig. 5), suggests anoxic/reducing conditions and high lake water levels (Fig. 15, Fig. 16). The limonite content, which increases as the age of the strata decreases, is mainly found in J_2t^2, J_2t^3 and J_3q (Fig. 6, Fig. 7), indicating that the dominant oxidizing conditions become more intense as the age of strata decreases (Fig. 15,Fig. 16).

5.2 Palaeo-salinity and Palaeoclimate

Strontium (Sr) and barium (Ba) can provide evidence for palaeo-salinity because the Sr/Ba ratio generally increases as the salinity of ambient water increases (Epstein and Mayeda, 1953; Cao et al., 2015; Moradi et al., 2016; Zhang et al., 2017). The Sr/Ba ratios of the Shishugou Group samples vary from 0.34 to 0.62, with an average of 0.48, indicating that the lake was filled with slight-medium salinity water during deposition (Table 2, Fig. 8j) (Zhang et al., 2017). Furthermore, the increasing Sr/Ba ratio of the Shishugou Group suggests that the slight-medium salinity of lake water changed over time (Table 2, Fig. 8j).

The climate can influence the geochemical signatures of sediments by its controls on the exogenic processes and terrigenous sediment flux into lacustrine environments (Tanaka et al., 2007; Meng et al., 2012; Bai et al., 2015). Therefore, the geochemical signatures of samples may provide evidence of palaeoclimatic conditions present during the deposition of the sediment (Worash, 2002). The Rb/Sr and Sr/Cu ratios of sediments are important indicators of palaeoclimatic conditions (Bai et al., 2015; Moradi et al., 2016). Substantially high ratios of Rb/Sr (0.44~1.14, average 0.81) of the samples demonstrate semiarid or arid conditions during deposition of the Shishugou

Group (Table 2, Fig. 8h, Fig. 15, Fig. 16,Fig. 17, Fig. 18).

The Sr/Cu ratios that range from 1.3 to 5 represent a warm-humid climate, while ratios over 5 indicate a hot-arid climate (Lerman, 1978). The Sr/Cu ratios of the mudstone in J_2t range nearly from 1 to 6 (av. 4.22), indicating a warm humid-hot arid climate condition (Table 2, Fig. 8i, Fig. 16, Fig. 17, Fig. 18). The Sr/Cu ratios of J_3q mudstone are clearly higher than 5, which suggests a hot arid climate condition (Table 2, Fig. 8i, Fig. 16, Fig. 17, Fig. 18). Therefore, the change in the Sr/Cu ratio can be interpreted as a change in palaeoclimate from warm-humid to hot-arid conditions (Table 2, Fig. 8i, Fig. 16, Fig. 17, Fig. 18). In addition, the abundance of the drought-enduring Gymnospermae classopollis within the Shishugou Group also indicates that the palaeo-climate was hot and arid as a whole (Fig. 18) (Zhu et al., 2017). The salinity change of lake water closely corresponds to the palaeoclimate changes, because climate change generally exerts a significant effect on the salinity of lake water by evaporation and atmospheric rainfall (Fig. 18).

5.3 Provenance

The Shishugou Group has three main provenances, including northeastern ,eastern Beisantai and southern sediment sources in the Fukang Sag (Zhang et al.,1999;Ji et al., 2014; Zou et al., 2014; Gong, 2015; Zhu et al., 2017). The dominant northeastern provenance from Kelameili Mountain consists of dominantly volcanic rock fragments, with minor amounts of metamorphic rock fragments (Fig. 1B) (Ji et al., 2014; Zou et al., 2014). Moreover, some previous researches show that both the eastern Beisantai and northeastern provenances might be derived from Kelameili Mountain (Shang et al.,2011; Ji et al.,2014). According to thin section analysis of rock samples from the field, the southern sediment source of the Tianshan Mountains (Bogeda Shan) is characterized by the dominance of metamorphic rock fragments, with minor contributions of volcanic rock fragments, although volcanic rock fragments are slightly more prevalent than metamorphic rock fragments in the early deposition of the Toutunhe Formation (Fig. 3g-l). The lithological change from conglomerate to medium sandstone in the field outcrop indicates the decreasing supply capacity of the southern provenance (Fig. 3g-l).

The ZTR values obviously vary in different members sandstone (J_2t^1, J_2t^2, J_2t^3, J_3q) of the Shishugou Group, which generally indicate some changes of provenances in study area during deposition (Fig. 15). Besides, the epidote content distribution, the 3-D seismic slices, ZTR and previous published result (Zhang et al.,1999) show that the sediments of J_2t^1 mainly came from the northeastern and southern provenances, the J_2t^2 and J_2t^3 derived from northeastern, southern and eastern (Beisantai heave) provenances, the J_3q derived from northeastern and eastern (Beisantai heave) sediment sources (Fig. 15). The supply range of southern provenance gradually decreased during deposition process in the south-eastern of study area (eastern Fukang slope) (Fig. 15). The 3-D seismic slices and uplift of North Santai heave demonstrate that the supply capacity of eastern provenance increased during the deposition of Toutunhe Formation (Fig. 15) (Zhang et al.,1999).

However, some research indicates that the eastern provenance (Beisantai) came from the north of Beisantai but not the Beisantai heave (Shang et al.,2011). Moreover, the eastern provenance (Beisantai) started to provide sediments for the Fukang Sag during the deposition of J_2t^2 (Fig. 15a-b). Therefore, the mother rock of eastern provenance probably came from the J_2t^1 sediments of Beisantai and Kelamei Mountain. The relative abundances of the remaining heavy minerals largely unaffected by the specific transport, deposition and burial processes, provided information on similar hydraulic and diagenetic behaviour (Morton and Hallsworth, 1999). Epidote is not only typically regarded as metamorphic minerals of igneous granitoid rocks but also the magmatic minerals originated from Plutons (Zen and Hammarstrom,1984), so the relative content of epidote provided important information about the provenance of the sediments. The heavy minerals of Shishugou Group sandstones, which mainly comprise the epidote, limonite and barite, indicate that the mother rock types of provenance were relatively simple and related with volcanic rocks and metamorphic rocks. Rare earth elements (REEs) are significant indicators of provenance because they are not extensively redistributed during transport, deposition and post-depositional processes (Nelson and DePaolo, 1988; McLennan, 1989; Liu et al., 2018). The almost-flat REE patterns with La_N/Yb_N values varying from 0.8 to 1.35 and averaging 1.06 indicate that the sediment source of the Shishugou Group is almost entirely from the same provenance (Table 3) (Fig. 9). Few samples show an obvious enrichment of Ce, which may be related to the partial redox conditions (Fig. 9). These indicate that the mother rocks of both northeastern and eastern (Beisantai heave) provenance came from the Kelameili Mountain and the southern provenance was very limited in the fourth region of central Junggar basin.

The petrology, heavy mineral distribution, 3-D seismic slices and geological setting suggest that the Kelameili Mountain provenance including northeastern and eastern provenances, influenced the greatest range of the sediments in the Fukang Sag, and the southern provenance, the Tianshan Mountains (Bogeda Shan), supplied sediments for only a very limited area of the southeastern Fukang Sag (Fig. 3a-i, Fig. 15 a-d). The supply area of the southern provenance decreased as the piedmont Sag developed, generated by the fast uplift of Bogda Shan during the deposition of Shishugou Group (Fig. 15a-d). Uplift of North Santai heave and south steep slope generated by fast uplift of Bogda Shan restricted the supply range of south provenance, especially in the fourth region of central Junggar Basin (Shang et al., 2011; Gong,2015), which can be explained by the alluvial fans of Toutunhe Formation in front of the Bogda Mountain (Fig. 3g). The rate and degree of chemical weathering on continents are mainly controlled by moisture and temperature conditions related to the climate, so a warm and humid climate may favour chemical weathering (Nesbitt and Young, 1982; Yan et al., 2007). The climate change from humid to hot and arid conditions may reduce the weathering rates and supply capacity of sediment provenance (Fig. 18) (Algeo and Twitchett, 2010; Liu et al., 2018).

5.4 Characteristics and evolution of sedimentary facies

The progradation, mouth bar and reverse rhythm，which are typical characteristics of the normal delta, were rarely observed in the shallow-water meandering river delta (Fig. 12, Fig. 13; Fig. 15, Fig. 16). The sandstone mainly consists of siltstone and fine sandstone (Fig. 11, Fig. 12, Fig. 13, Fig. 14). The green-grey, brown and brownish-red mudstone were pervasive in the shallow-water meandering river delta facies (Fig. 11, Fig. 12, Fig. 13, Fig. 14, Fig. 16).Obviously, the granularity size of sandstone of shallow-water meandering river delta is generally less than normal delta, but the oxide colours of mudstone are very pervasive in the shallow-water delta. The sedimentary structures include parallel bedding, current bedding, cross-bedding and basal erosional scour structures in the shallow-water delta. The shallow-water meandering river delta sedimentary succession has a large overall thickness but relatively thin single-layer sand bodies (1-15 m, av.3m) and relatively low sand-strata ratios (0.2-0.55), which are obviously less than that of the normal delta (Fig. 11, Fig. 12, Fig. 13, Fig. 14). The meandering river facies are characterized by the thin, fine-medium grained point bar sandstones and a lack of marsh deposits (Fig. 15, Fig. 16, Fig. 17).

During deposition of J_2t^1, the sedimentary environment consisted of lake and shallow-water meandering river delta front. The sedimentary facies of J_2t^1 are characterized by the “big front-small plain” delta (BFBPD), which dominantly comprise the shallow-water meandering river delta front with minor constituents of a shallow-water meandering river delta plain (Fig. 15a, Fig. 16a, Fig. 17a, Fig. 18). The plain range of J_2t^2 increased in comparison with the J_2t^1 (Fig. 15b, Fig. 16b). Conversely, the depositional facies of J_2t^3 is the “big plain-small front” delta (BPBFD), which dominantly consists of a shallow-water meandering river delta plain environment with minor shallow-water meandering river delta front constituents (Fig. 15c, Fig. 16c, Fig. 17b, Fig. 18). Therefore, the shallow-water meandering river delta plain environment rapidly transformed into a meandering river environment during the deposition of J_3q (Fig. 15d, Fig. 16d, Fig. 17c, Fig. 18).

5.5 The relationships among palaeo-environment, provenance and sedimentary systems

The gentle slope structure, climate condition, lake level change and stable provenance are necessary conditions and controlling factors of the development of shallow water delta (Zhu et a.,2012; Zhu et al.,2013).

The semiarid-hot arid climate and the continuous uplift of the Bogeda Shan and Kelameili Shan may cause reductions in lake level and lake range (Fig. 15, Fig. 16, Fig. 17; Fig. 18). Moreover, the redox condition changed from weak anoxic/oxic conditions to intensive oxidizing conditions in response to changes in palaeosalinity, palaeoclimate and lake level (Fig. 18). Therefore, the lake gradually shrank from the centre to southwest of Fukang Sag during deposition of the Shishugou Group (Fig. 15, Fig. 16). The sedimentary system had never significantly changed due to the stable Kelameili Mountain provenance. The alluvial fans of Toutunhe Formation were only found in the front of Bogda Mountain because of the limited supply range of south provenance (Fig. 15, Fig. 16).

The west-southward gentle slope of the Fukang Sag, the relatively far Kelameili Mountain provenance, the warm humid-hot arid climate condition and the low lake level were beneficial to the development of a meandering river and shallow-water meandering river delta (Fig. 15, Fig. 16, Fig. 18) (Postma, 1990; Lemons and Chan, 1999; Hoy and Ridgway, 2003; Cornel and Janok, 2006; Zhu et al., 2012; Zhu et al., 2016). The gentle slope is the primary condition necessary for the formation of a shallow-water meandering river delta. The palaeo-environment and provenance play a critical role in the development and evolution of a shallow-water meandering river delta (Fig. 16, Fig. 18).

The shallow-water meandering river delta can be divided into the humid delta and the hot arid delta according to the climate conditions present (Zhu et al., 2012; Zhu et al., 2016).The humid shallow-water delta is characterised by a “big front-small plain” delta (BFBPD)(Fig. 16a) and the hot arid delta is characterized by a “big plain-small front” delta (BPBFD) (Fig. 16b) (Zhu et al., 2012; Zhu et al., 2016). Therefore, the depositional evolution from the “big front-small plain” shallow-water delta (BFBPD) to the “big plain-small front” shallow-water delta (BPBFD) was controlled by the change in climate and supply capacity of the sediment provenance (Fig. 16, Fig. 18). The shallow-water meandering-river delta-plain environment rapidly changed into a meandering river environment during the deposition of J_3q, which can be interpreted to indicate that the hot arid climate conditions markedly reduced the lake level, lake range and supply capacity of the sediment provenance (Fig. 16b-c, Fig. 18).

6. Conclusions

1. The redox conditions changed from weak anoxic/oxic into strong oxic conditions during the deposition of the Middle-Late Jurassic Shishugou Group. The dominant

oxidizing conditions became more intense as strata age decreased.

2. The climate changed from warm-humid to hot-arid during the Middle-Late Jurassic in the Junggar Basin, which may have increased the salinity of the lake water and reduced the supply capacity of the sediment provenance.

3. The Kelameili Mountain provenance comprising northeastern and eastern Beisantai provenances, is the most important sediment source, but the south provenance, the Tianshan Mountains, (Bogeda Shan) supply sediments only for the very limited area of the southeastern Fukang Sag.

4. The gentle slope is the primary condition necessary for the formation of lake-shallow water delta-meandering river sedimentary systems, especially the shallow-water meandering river delta. The palaeo-environment and provenance play critical roles in the development and evolution of lake-shallow water delta-meandering river sedimentary systems.

Acknowledgement

We greatly thank the Western Research Institute, Shengli Oilfield Branch Company of Sinopec for providing all the related core samples, geological data and permission to publish these data. This work was funded by the Major Special Project for National Science and Technology [Grant numbers. 2016ZX05033-001-002], National Natural Science Foundation of China [Grant numbers. 41202043], and the China Scholarship Council (CSC). Finally, we especially thank the editors and reviewers for their work in improving the manuscript.

References

Algeo, T.J., ＆ Twitchett, R.J. (2010). Anomalous Early Triassic sediment fluxes due to elevated weathering rates and their biological consequences. Geology, 38 (11), 1023–1026.

Algeo, T.J., Hinnov, L., Moser, J., Maynard, J.B., Elswick, E., Kuwahara, K., ＆ Sano, H. (2010). Changes in productivity and redox conditions in the Panthalassic Ocean during the latest

Permian. Geology, 38 (2), 187–190.

Aubrecht, R., Sýkora, M., Uher, P., Li, X., Yang, Y., Putiš, M., ＆ Plašienka, D. (2017). Provenance of the Lunz Formation (Carnian) in the Western Carpathians, Slovakia: Heavy mineral study and in situ LA–ICP–MS U–Pb detrital zircon dating. Palaeogeography, Palaeoclimatology, Palaeoecology ,471, 233-253.

Bai, Y., Liu, Z., Sun, P., Liu, R., Hu, X., Zhao, H., ＆ Xu, Y. (2015). Rare earth and major element geochemistry of Eocene fine-grained sediments in oil shale- and coal-bearing layers of the Meihe Basin, northeast China. Journal of African Earth Sciences， 97 (A)， 89–101.

Baioumy, H., ＆ Lehmann, B. (2017). Anomalous enrichment of redox-sensitive trace elements in the marine black shales from the Duwi Formation, Egypt: Evidence for the late Cretaceous Tethys anoxia. Journal of African Earth Sciences, 133, 7-14.

Bassis, A., Hinderer,M., ＆ Meinhold,G. (2016). New insights into the provenance of Saudi Arabian Palaeozoic sandstones from heavy mineral analysis and single-grain geochemistry Sedimentary Geology, 333, 100-114.

Berner, R.A. (1994). GEOCARBⅡ: a revised model of atmospheric CO2 over Phanerozoic time. American Journal of Socience, 294, 56-91.

Bhatia, M.R. (1983). Plate tectonics and geochemical composition of sandstones. Journal of Geology, 91, 611–627.

Bhatia, M.R., ＆Crook, K.A. (1986). Trace element characteristics of graywackes and tectonic setting discrimination of sedimentary basins. Contributions to Mineralogy and Petrology, 92, 181–193.

Cao, J., Wu, M., Chan, Y., Hu, K., Bian, L. Z., Wang, L.G., ＆ Zhang, Y. (2012). Trace and rare earth elements geochemistry of Jurassic mudstones in the northern Qaidam basin, northwest China. Chemie der Erde, 72, 245–252.

Cornel, O., ＆ Janok, P.B. (2006). Terminal distributary channels and delta front architecture of river dominated delta systems. Journal of Sedimentary Research, 76, 212-233.

Cross, T. A. (1994). High-resolution stratigraphic correlation from the perspective of base-level cycles and sediment accommodation. In: Proceeding of Northwestern European Sequence

stratigraphy Congress, 105-123.
Cullers, R.L. (1995). The controls on the major- and trace-element evolution of shales,siltstones and sandstones of Ordovician to Tertiary age in the wet mountains region,Colorado, USA. Chemical Geology, 123, 107–131.
Deng, S., Lu, Y., Zhao, Y., Fan, R., Wang, Y., Yang, X., Li, X., ＆ Sun, B. (2017). The Jurassic palaeoclimate regionalization and evolution of China. Earth Science Frontiers, 24,106-142 (in Chinese with English Abstract).
Dickinson, W.R., ＆ Suczek, C.A. (1979). Plate tectonics and sandstone compositions. AAPG Bulletin, 63, 2164–2182.
Dinis, P.A., ＆ Soares, A.F. (2007). Stable and ultrastable heavy minerals of alluvial to nearshore marine sediments from Central Portugal: Facies related trends. Sedimentary Geology, 201, 1-20.
Do Campo, M., Del Papa, C., Jiménez-Millán, J., ＆ Nieto, F. (2007). Clay mineral assemblages and analcime formation in a Palaeogene fluvial-lacustrine sequence (Maíz Gordo Formation Palaeogen) from northwestern Argentina. Sedimentary Geology, 201, 56–74.
Do Nascimento Jr, D.R., Sawakuchi, A.O., Guedes, C.C.F., Giannini, P.C.F., Grohmann, C.H., ＆ Ferreira, M.P. (2015). Provenance of sands from the confluence of the Amazon and Madeira rivers based on detrital heavy minerals and luminescence of quartz and feldspar. Sedimentary Geology, 316,1-12.
El-Sabbagh, A.M., El-Hedeny, M.M., ＆ Mansour, A.S. (2017). Palaeoecology and palaeoenvironment of the Middle–Upper Jurassic sedimentary succession, central Saudi Arabia. Proceedings of the Geologists' Association, 128, 340-359.
Engelmanna, F. G., Chureb, J.D., ＆ Fiorillo, R. A. (2004). The implications of a dry climate for the palaeoecology of the fauna of the Upper Jurassic Morrison Formation. Sedimentary Geology, 167, 297-308.
English, P.M. (2001). Formation of analcime and moganite at Lake Lewis, central Australia: significance of groundwater evolution in diagenesis. Sedimentary Geology, 143,219–244.
Fisk, H. N. (1954). Sedimentary framework of the modern Mississippi delta. Journal of Sedimentary

Petrology, 24(2):76-99.

Floyd, P.A., Keele, B.E., Leveridge, B.E., Franke,W., Shail, R., & Dörr, W. (1990). Provenance and depositional environment of Rhenohercynian synorogenic greywackes from the Giessen Nappe, Germany. Geologische Rundschau, 79 (3), 611–626.

Galarragaa, F., Reateguia, K., Martïneza, A., Martíneza,M., Llamas,J,F., & Márquez,G.(2008). V/Ni ratio as a parameter in palaeoenvironmental characterisation of nonmature medium-crude oils from several Latin American basins. Journal of Petroleum Science and Engineering,61,9-14.

Galloway, J.M., Sweet, A.R., Swindles, G. T., & Dewing, K. (2013). Middle Jurassic to Lower Cretaceous palaeoclimate of Sverdrup Basin, Canadian Arctic Archipelago inferred from the palynostratigraphy. Marine and Petroleum Geology, 44, 240-255.

Garzanti, E., Andò, S., & Vezzoli, G. (2008). Settling-equivalence of detrital minerals and grain size dependence of sediment composition. Earth and Planetary Science Letters, 273, 138–151.

Gong, Q. (2015). Sedimentary characteristics and tectonic background of the Jurassic in the south and east margin of the Junggar basin. (Master thesis) China University of geosciences, Beijing, China, 59-62 (in Chinese with English Abstract).

Graver, J.I., &and Scott, T.J. (1995). Trace elements in shale as indicators of crustal province and terrain accretion in the southern Canadian Cordillera. Geological Society of America Bulletin, 107, 440–453.

Greene, T. J., Carroll, A. R., Hendrix, M. S., Graham, S.A., & Warters, M.A. (2001). Sedimentary record of Mesozoic deformation and inception of the Turpan-Hami basin, northwest China. In: Hendrix, M.S., Davis, G. A. (Eds.), Palaeozoic and Mesozoic Tectonic Evolution of Central Asia: From continental assembly to intracontinental deformation. Geological Society of America Memoir, 194,317-340.

Grome, L.P., Haskin,L.A., Korotev , R. L., &Dymek, R. F.,(1984). The “North American shale composite”: Its compilation, major and trace element characteristics. Geochimica et Cosmochimica Acta,48(12),2469-2482. Harrell, JR.T. L & Pe´rez-Huerta, A. (2015). Rare Earth elements (REE) analysis of vertebrate fossils from the Upper Cretaceous Carbonate marine formations of western and central Alabama, USA: Taphonomic and Paleoenvironmental implications. PALAIOS, 30,514-528.

Hartley, A., Flint, S., ＆ Turner, P. (1991). Analcime: a characteristic authigenic phase of Andean alluvium, northern Chile. Geological Journal, 26, 189–202.

Hoy, R.G., ＆ Ridgway, K.D. (2003). Sedimentology and sequence stratigraphy of fan delta and river delta deposystems, Pennsylva-nian Minturn Formation, Colorado. AAPG Bulletin, 87 (7), 1169-1191.

Huber, B.T., MacLeod, K. G., ＆ Wing, S.T. (2000). Warm Climates in Earth History. Cambridge University Press, Cambridge.

Ji, J., Wen, H., Xiang, B., Qi, L., Yu, J., ＆ Li, L. (2014). Provenance analysis of Middle Jurassic Toutunhe Formationin eastern Fukang slope, Junggar Basin. Lithological Reservoir, 26(2), 54-59(in Chinese with English abstract).

Jin, B., Lin, Z., Yang, Q., ＆ Ji, F. (2002). Application of sedimentary mineralogy to the environmental analysis in marginal seas. Marine Geology & Quaternary Geology, 22(3), 113-118.

Jone, J. S., Arzani, N., ＆ Allen, B.M. (2014). Tectonic and climatic controls on fan systems: The Kohrudmountain belt,Central Iran. Sedimentary Geology, 302, 29-43.

Jones, B., ＆Manning, D. A. C. (1994). Comparison of geochemical indices used for the interpretation of palaeoredox conditions in ancient mudstones. Chemical Geology ,111,111-129.

Kim, B., Cheong, D., ＆Lee, E. (2015). Palaeoenvironmental changes in northern Mongolia during the last deglaciation revealed by trace element records in ostracods from Lake Hovsgol. Quaternary International, 384,169-179.

Kuzyk, Z.Z.A., Gobeil,C., Goni, M. A., ＆ Macdonald, R.W. (2016). Early diagenesis and trace element accumulation in North American Arctic margin sediments. Geochimica et Cosmochimica Acta, 203, 175-200.

Lemons, D. R., ＆Chan, M. A . (1999) .Facies architecture and sequence stratigraphy of fine-grained lacustrine deltas along the eastern margin of late Pleistocene Lake Bonneville，northern

Utah and southern Idaho. AAPG Bulletin，83(4) : 635-665.

Lee, Y.I. (2009). Geochemistry of shales of the Upper Cretaceous Hayang Group, SE Korea: implications for provenance and source weathering at an active continental margin. Sedimentary Geology, 215, 1–12.

Lemons, D.R., ＆ Chan, M.A. (1999). Facies architecture and sequence stratigraphy of fine grained lacustrine deltas along the eastern margin of late Pleistocene Lake Bonneville, northern Utah and southern Idaho. AAPG Bulletin, 83 (4), 635-665.

Lerman, A. (1978). Chemistry, Geology and Physics of Lake. Springer- Verlag, New York, Heidelberg Berilin.

Li, P., Zou, H., ＆ Hao, F. (2006). Formation Mechanism and effect on petroleum accumulation of the weathering crust top of Jurassic in the Hinterland of Junggar Basin. Acta Sedimentolohica Sinica, 24(6), 889-896 (in Chinese with English abstract).

Lin, Z., Chen, D., ＆ Liu, Q. (2008). Geochemical indices for redox conditions of marine sediments. Bull. Mineral. Petrology and Geochemistry, 27(1), 72-80.

Liu, D., Kong, X., Zhang, C., Wang, J., Yang, D., Liu, X., Wang, X., ＆ Song, Y. (2018). Provenance and geochemistry of Lower to Middle Permian strata in the southern Junggar and Turpan basins: A terrestrial record from mid-latitude NE Pangea. Palaeogeography, Palaeoclimatology, Palaeoecology, 495, 259-277.

Liu, Y. (2012). Lower Jurassic heavy minerals from southern Mt. Hala'alate，Junggar Basin: Characteristics and geological implications. Sedimentary Geology and Tethyan Geology, 32(4): 34-37.

Luo, L., Gao, X., Meng, W., Tan, X., Shao, H., ＆ Xiao, C. (2018). The origin and alteration of calcite cement in tight sandstones of Jurassic Shishugou Group in the Fukang Sag, Junggar Basin, NW China: Implications for fluid–rock interactions and porosity evolution. Australian Journal of Earth Sciences, 65(3),427-445.

Lv, D., ＆Chen, J. (2014). Depositional environments and sequence stratigraphy of the Late Carboniferous - Early Permian coal-bearing successions (Shandong Province, China): Sequence development in an epicontinental basin. Journal of African Earth Sciences, 79, 16-

30.

Lv,D., Zong, R., Li, Z., Wang, D., Liu, H., Wu, X., Wang, X., Yu, D., Feng, T., Zhao, L., Yang, Q., & Yong, P. (2016).Oil shale paleo-productivity disturbed by sea water in a coal and oil shale bearing succession: A case study from the Paleogene Huangxian basin of Eastern China. Journal of Petroleum Science and Engineering, 139, 62-70.

Lv, D., Wang, D., Li, Z., Liu, H., & Li, Y. (2017). Depositional environment, sequence stratigraphy and sedimentary mineralization mechanism in the coal bed- and oil shale-bearing succession: A case from the Paleogene Huangxian Basin of China. Journal of Petroleum Science and Engineering 148: 32-51.

Martínez-Yáñez, M., Núñez-Useche,F., & Martínez,R.L.(2017). Palaeoenvironmental conditions across the Jurassic–Cretaceous boundary in central-eastern Mexico. Journal of South American Earth Sciences, 77, 261-275.

McCulloch, M.T., & Wasserburg, G.J. (1978). Sm–Nd and Rb–Sr chronology of continental crust formation. Science, 200, 1003–1011.

McLennan, S.M., & Taylor, S.R. (1991). Sedimentary rocks and crustal evolution: tectonic setting and secular trends. Journal of Geology, 99,1–21.

McLennan, S.M., Taylor, S.R., & Eriksson, K.A. (1983). Geochemistry of Archean shales from the Pilbara Supergroup, Western Australia. Geochimica et Cosmochimica Acta, 47,1211–1222.

McLennan, S.M., Hemming, S., McDaniel, D.K., & Hanson, G.N. (1993). Geochemical approaches to sedimentation, provenance, and tectonics. Geological Society of America Special Papers, 284, 21–40.

Meng, Q.T., Liu, Z.J., Bruch, A.A., Liu,R., & Hu, F. (2012). Palaeoclimatic evolution during the Eocene and its influence on oil shale mineralisation, Fushun Basin, China. Journal of African Earth Sciences, 45, 95 – 105.

Moore, G.T., Hayashida, D.N., Ross, C.A., & Jacobson, S. R. (1992).Palaeoclimate of the Kimmeridgian/Tithonian (Late Jurassic) world: I. Results using a general circulation model. Palaeogeography, Palaeoclimatology, Palaeoecology, 93,113-150.

Moradi, A.V., Sarı, A., & Akkaya, P. (2016). Geochemistry of the Miocene oil shale (Hançili

Formation) in the Çankırı-Çorum Basin, Central Turkey: Implications for Palaeoclimate conditions, source–area weathering, provenance and tectonic setting. Sedimentary Geology, 341, 289–303.

Moreno, C.J., Caballero, V., & Parra, M. (2012). Integrated provenance analysis of a convergent retroarc foreland system: U–Pb ages, heavy minerals, Nd isotopes, and sandstone compositions of the Middle Magdalena Valley basin, northern Andes, Colombia. Earth-Science Reviews, 110,111–126.

Morton, A.C., & Hallsworth, C.R. (1999). Processes controlling the composition of heavy mineral assemblages in sandstone. Sedimentary Geology, 124, 3–29.

Morton, A.C., Meinhold,G., Howard,J.P., Phillips,R.J., Strogen,D., Abutarruma,Y., Elgadry,M., Thusu,B., & Whitham,A.G. (2011). A heavy mineral study of sandstones from the eastern Murzuq Basin, Libya: Constraints on provenance and stratigraphic correlation. Journal of African Earth Sciences, 61, 308-330.

Murray, R.W., Buchholtz ten Brink, M.R., Gerlach, D.C., Russ,D.P., & Jones, D.L. (1992). Interoceanic variation in the rare earth, major, and trace element depositional chemistry of chert: Perspectives gained from the DSDP and ODP record. Geochimica et Cosmochimica Acta, 56, 1897–1913.

Murthy, R., Kidder, D., Mapes, R., & Hannigan, R. (2004). Rare-earth element chemistry of Mississippian–age phosphate nodules in the Fayetteville Shale of Oklahoma and Arkansas. Environmental Geosciences, 11(2), 99-111.

Myers, T.S., Tabor, N.J., & Jacobs, L.L. (2011). Late Jurassic palaeoclimate of Central Africa. Palaeogeography, Palaeoclimatology, Palaeoecology, 311(1-2), 111-125.

Nesbitt, H.W., & Young, G.M. (1982). Early Proterozoic climates and plate motions inferred from major element chemistry of lutites. Nature, 299, 715–717.

Nie, J.S., Horton, B.K., Saylor, J.E., Mora, A., Mange, M., Garzione, C.N., Basu, A.,Moreno, C.J., Caballero, V., & Parra, M. (2012). Integrated provenance analysis of a convergent retroarc foreland system: U–Pb ages, heavy minerals, Nd isotopes, and sandstone compositions of the Middle Magdalena Valley basin, northern Andes, Colombia. Earth-Science Reviews, 110, 111–

126.

Owen, A.W., Armstrong, H.A., ＆ Floyd, J. D. (1999).Rare earth elements in chert clasts as provenance indicators in the Ordovician and Silurian of the Southern Uplands of Scotland. Sedimentary Geology, 124,185-195.

Pi, D.H., Jiang, S.Y., Luo, L., Yang, J.H., ＆ Ling, H.F. (2014). Depositional environments for stratiformwitherite deposits in the Lower Cambrian black shale sequence of the Yangtze Platform, southern Qinling region, SWChina: evidence from redox-sensitive trace element geochemistry. Palaeogeography, Palaeoclimatology, Palaeoecology, 398, 125-131.

Postma, G. (1990). An analysis of the variation in delta architecture. Terra Nova 2(2), 124-130.

Potter-McIntyre, S.L., Boraas, M., DePriest,K., ＆ Aslan,A. (2016).Middle Jurassic landscape evolution of southwest Laurentia using detrital zircon geochronology. Lithosphere, 8,185-193.

Rimstidt, J.D., Chermak, J.A., ＆ Schreiber, M.E. (2017). Processes that control mineral and element abundances in shales. Earth-Science Reviews, 171, 383-399.

Roser, B.P., ＆ Korsch, R.J. (1986). Determination of tectonic setting of sandstone–mudstone suites using SiO2 content and K2O/Na2O ratio. Journal of Geology, 94, 635–650.

Sellwood, B.W., ＆ Valdes, P.J. (2008). Jurassic climates. Proceedings of the Geologists Association, 119, 5-17.

Sevastjanova, I., Hall, R., ＆ Alderton, D. (2012). A detrital heavy mineral viewpoint on sediment provenance and tropical weathering in SE Asia. Sedimentary Geology, 280,179-194.

Shang, L., Dai, J., Liu,X., ＆Bian,B.(2011). Sedimentary source analysis of Jurassic Toutunhe Formation in Beisantai area in Junggar Basin. Global Geology,30(4),579-584(in Chinese with English abstract).

Sochava, A.V., Podkovyrov, V.N., ＆ Felitsyn, S.B. (1994). Late Precambrian evolution of terrigenous rock composition. Stratigraphy and Geological Correlation, 2, 3–21.

Souto, P.R.F., ＆ Fernandes, M.A. (2017). Palaeobiogeographical significance of the Late Jurassic continental fauna from western Gondwana. Palaeoworld, 26, 230-240.

Su, Z., Chen, L., Xu, T., Zhang, M., Zhang, R., ＆Xiu, J. (2014). Provenance system research of

Jurassic Toutunhe Formation in 2,4 blocks of the middle of Junggar Basin. Petroleum Geology and Engineering, 28（2），9-11 (in Chinese with English abstract).

Svendsen,J.B., ＆ Hartley, N.R. (2002). Synthetic heavy minerals stratigraphy: applications and limitations. Marine and Petroleum Geology, 19, 389–405.

Sverjensky, D. A. (1984). Europium redox equilibria in aqueous solution. Earth and Planetary Science Letters, 67, 70–78.

Tan, M., Zhu, X., Geng, M., Zhu, S., ＆ Liu, W. (2017). The occurrence and transformation of lacustrine sediment gravity flow related to depositional variation and paleoclimate in the Lower Cretaceous Prosopis Formation of the Bongor Basin, Chad. Journal of African Earth Sciences, 134, 134-148.

Tanaka, K., Akagawa, F., Yamamoto, K., Tani, Y., Kawabe, I., ＆ Kawai, T. (2007). Rare earth element geochemistry of Lake Baikal sediment: its implication for geochemical response to climate change during the Last Glacial/Interglacial transition. Quaternary Science Reviews, 26 (9), 1362–1368.

Tribovillard, N., Algeo, T. J., Lyons, T., ＆ Riboulleau, A. (2006). Trace metals as palaeoredox and palaeoproductivity proxies –An update. Chemical Geology, 232,12 -32.

Vernet, J.P. (1961). Concerning the association montmorillonite–analcime in the series of Stanleyville, Congo. Journal of Sedimentary Research, 31 (2), 293–295.

Wang, X., Hou, J., Song, S., Wang, D., Gong, L., Ma, K., Liu, Y., Li, Y., ＆ Yan, L. (2018). Combining pressure-controlled porosimetry and rate-controlled porosimetry to investigate the fractal characteristics of full-range pores in tight oil reservoirs. Journal of Petroleum Science and Engineering, 171, 353-361.

Wang, Y., Wang, Y., Qi, X., Guan, S., Zhao, X., ＆ Li, R. (2001). Classification of stratigraphic sequences of Jurassic in Junggar Basin. Xinjiang Petroleum Geology, 22(5), 382-385.

Wierzbowski, H., Rogov, M.A., Matyja, B.A., Kiselev, D., ＆ Ippolitov, A. (2013). Middle–Upper Jurassic (Upper Callovian–Lower Kimmeridgian) stable isotope and elemental records of the Russian Platform: Indices of oceanographic and climatic changes. Global and Planetary Change, 107, 196-212.

Wignall, P.B., ＆ Twitchett, R.J. (1996). Oceanic anoxia and the end Permian mass extinction. Science, 272, 1155-1158.

Wilde, P., Quibabyhunt, M. S., ＆Erdtmann, B. D.,1996. The whole-rock Cerium anomaly : A potential indicator eustatic sea-level changes in shales of anoxic facies. Sedimentary Geology, 101，43-53.

Worash, G. (2002). Geochemistry provenance and tectonic setting of the Adigrat sandstone northern Ethiopia. Journal of African Earth Sciences, 35, 185–198.

Wu, Q. (1986). Development stage tectonic units and origin of local structure of Junggar Basin. Xinjiang Petroleum Geology, 7(1), 29-37 (in Chinese with English abstract).

Yan, Y., Xia, B., Lin, G., Cui, X., Hu, X., Yan, P., ＆ Zhang, F. (2007). Geochemistry of the sedimentary rocks from the Nanxiong Basin,South China and implications for provenance, palaeoenvironment and palaeoclimate at the K/T boundary. Sedimentary Geology, 197, 127-140.

Yu, J., Liu, N., Wen, H., Zhu, R., ＆ Zhang, Z. (2016). Analysis of high-resolution sequence stratigraphy and prediction of favorable sandbodies in the Upper Jurassic Qigu Formation in Fudong slope area，Junggar Basin. Journal of Palaeogeography, 18(2), 265-274 (in Chinese with English abstract).

Yu, J., Zheng, R., Qi, L., Zhang, Z., Wen, H., ＆ Li, Y.2014. Precise Analysis on High-resolution Sequence Stratigraphy and Micro-facies of Toutunhe Formation of Middle Jurassic in the East Slope Zone，Fukang Sag，Junggar Basin. Geological Review, 60(6), 1337-1347 (in Chinese with English abstract).

Zhang, B.M., Chen, J.P., Bian, L.Z., ＆ Zhang, S.C. (2006). Rediscussion on the sea-looding events during Triassic to Jurassic of Kuqa Depression in Tarim Basin. Acta Geol. Si Acta Geologica Sinica, 80, 236–244 (in Chinese with English abstract).

Zhang, Q., Zhang, M., Zhu, X., Zhong, D., ＆Wang, G. (1999). Analysis of Jurassic Sources in Fukang of Junggar Basin.Xinjiang Petroleum Geology, 20 (6),501-504 (in Chinese with English abstract).

Zhang, M., Zhang, Q., Zhu, X., Li, X., ＆ Wang, J. (2000). Sequence stratigraphy of Jurassic on the east Fukang slope,Junggar Basin. Journal of Palaeogeography, 2(3), 27-36 (in Chinese with English abstract).

Zhang, X., Lin, C., Zahid, M.A., Jia, X., ＆ Zhang, T. (2017).Palaeosalinity and water body type of Eocene Pinghu Formation, Xihu Depression, East China Sea Basin. Journal of Petroleum Science and Engineering, 158, 469-478.

Zhao, Z.Y., Zhao, J.H., Wang, H.J., Liao, J.D., ＆ Liu, C.M. (2007). Distribution characteristics and applications of trace elements in Junggar Basin. Natural Gas Exploration and Development, 30,30–33 (in Chinese with English abstract).

Zhu, X., Li, S., Wu, D., Zhu, S., Dong, Y., Zhao, D., Wang, X., ＆ Zhang, Q. (2017). Sedimentary characteristics of shallow-water braided delta of the Jurassic, Junggar basin, Western China Journal of Petroleum Science and Engineering, 149, 591-602.

Zhu, X., Pan, R., Zhao, D., Liu, F., Wu, D., Li, Y., ＆Wang, R. (2013). Formation and development of shallow-water deltas in lacustrine basin and typical case analyses. Journal of China University of Petroleum,37(5),7-14(in Chinese with English abstract).

Zhu, X., Liu, Y., Fang, Q., Li, Y., Liu, Y., Wang, R., Song, J., Liu, S., Cao, H., ＆ Liu, X. (2012). Formation and sedimentary model of shallow delta in large scale lake, example from Cretaceous Quantou Formation in Sanzhao Sag, Songliao Basin. Earth Science Frontiers, 19 (1), 089-099 (in Chinese with English abstract).

Zhu, X., Zhong, D., Yuan, X., Zhang, H., Zhu, S., Sun, H., Gao, Z., ＆ Xian, B. (2016). Development of sedimentary geology of petroliferous basins in China. Petroleum Exploration & Development, 43(5), 820-829 (in Chinese with English abstract).

Zou, Z., Yu, C., ＆ Chen, H. (2014). Sedimentary Characteristics of Toutunhe Formation 2nd Member on East Fukang Slope of Junggar Basin. Xinjiang Geology, 32(2), 214-218 (in Chinese with English abstract).

Figure captions

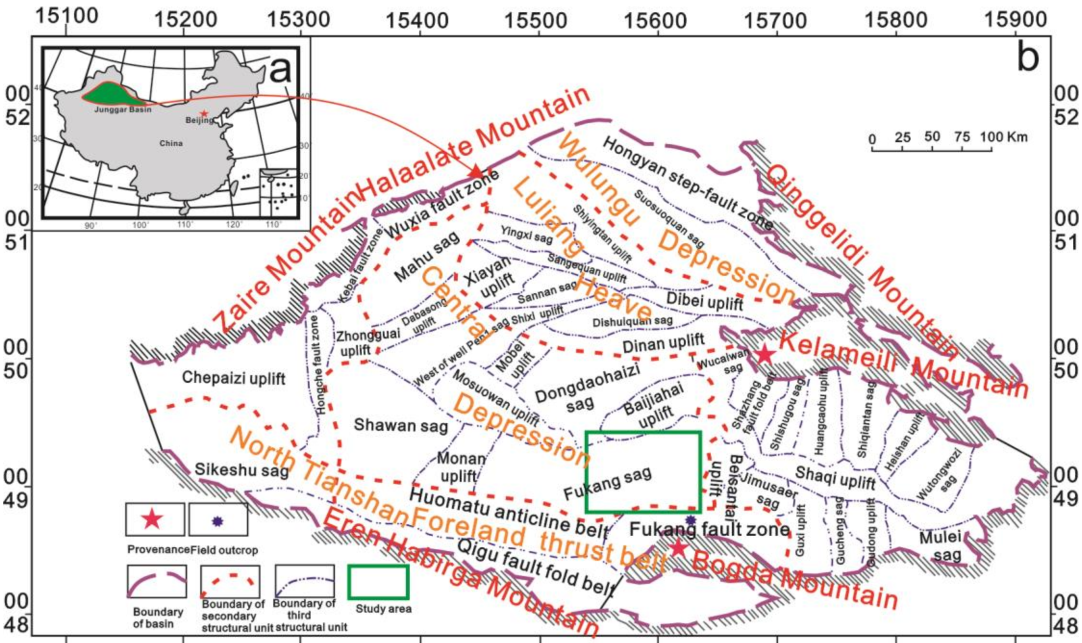

Fig. 1. Maps showing the (a) Location of the Junggar Basin in China and (b) Location of the Fukang Sag

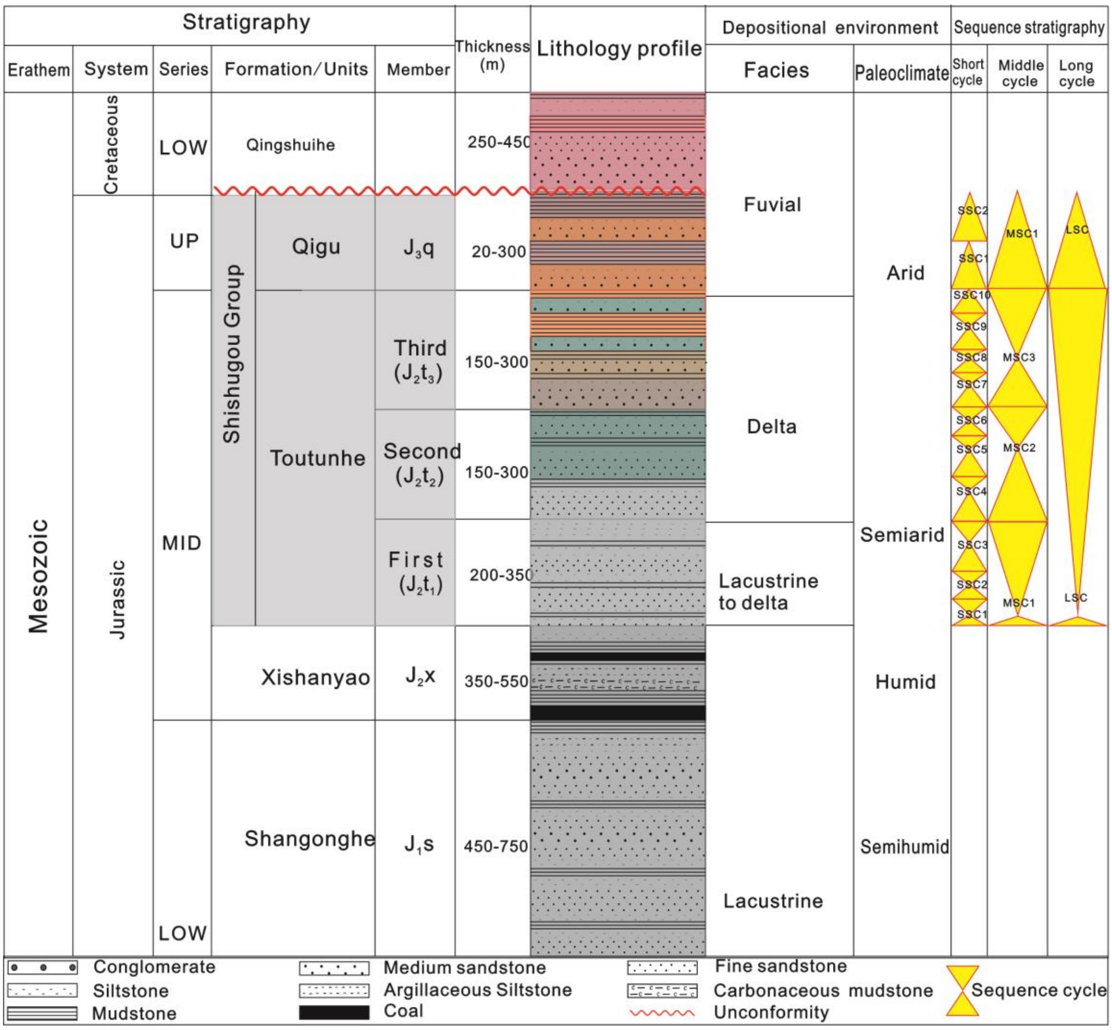

Fig. 2. Stratigraphic column of the Fukang Sag of Junggar Basin showing the Shishugou Group (the Toutunhe and Qigu Formations).

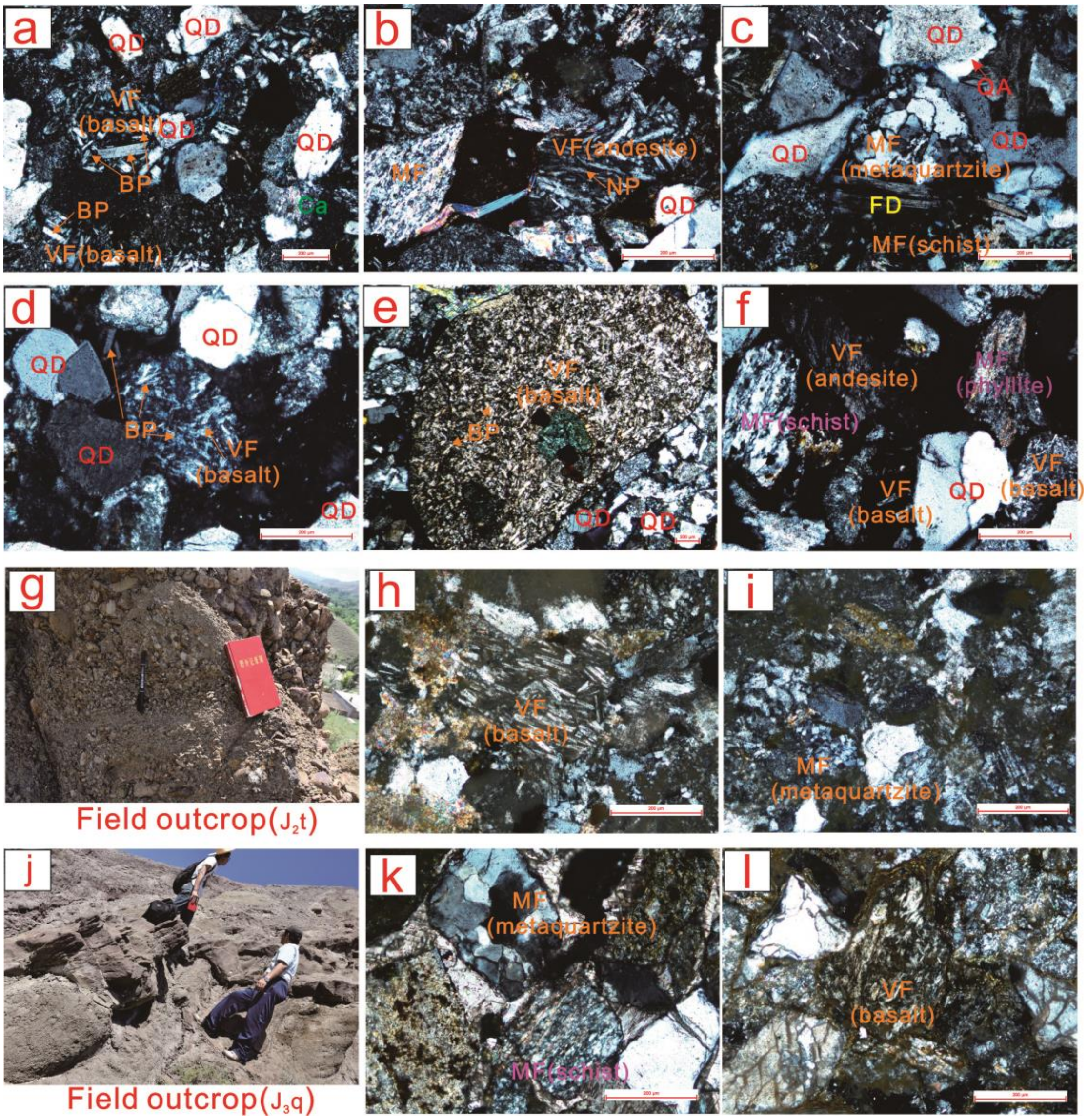

Fig. 3. Petrological and mineralogical characteristics of the Shishugou Group sandstone, detrital quartz -QD (based on Luo et al.,2018)：(A) Micrograph of thin section showing the volcanic rock fragment (VF) comprising basalt fragments characterized by porphyritic texture with bundles or radial pattern of lath-shaped basic plagioclase phenocryst (BP), well D7, 4517.6m, J_2t. (B) Micrograph of thin section showing andesite fragments (VF) characterized by porphyritic texture with directionally arranged neutral plagioclase phenocryst (NP),well D7,4133.4m, J_2t. (C) Micrograph of thin section showing the metamorphic rock fragment (MF) consisting of metaquartzite and schist , quartz

overgrowth (QA) and feldspar (FD),well D8,4545.4m, J_2t.(D) Micrograph of thin section showing the basalt fragments (VF) characterized by porphyritic texture with radial distribution of lath-shaped basic plagioclase phenocryst (BP), well D6, 4257.65m, J_3q. (E) Micrograph of thin section showing the basalt fragments (VF) characterized by porphyritic texture with radial distribution of lath-shaped basic plagioclase phenocryst (BP),well D701,3902.95m, J_3q. (F) Micrograph of thin section showing the volcanic rock fragment (VF) including basalt and andesite fragments and the metamorphic rock fragment (MF) comprising schist and phyllite, well D6,4257.65m, J_3q. (G) Photograph of conglomerate of the J_2t in the Sangonghe field outcrop (Fig. 1) showing existence of south provenance.(H) Micrograph of conglomerate collected from the outcrop of G showing that rock fragment comprising volcanic (basalt) rock fragment (VF). (I) Micrograph of conglomerate collected from the outcrop of G showing that rock fragment comprising metamorphic (Metaquartzite) rock fragment (MF). (J) Photograph of the J_3q in the Sangonghe field outcrop (Fig. 1) showing the channel deposit with sandstone lens. (K) Micrograph of sandstone collected from the outcrop of J showing that rock fragment comprising metamorphic (Metaquartzite) rock fragment (MF). (L) Micrograph of sandstone collected from the outcrop of J showing that rock fragment comprising volcanic (basalt) rock fragment (VF).

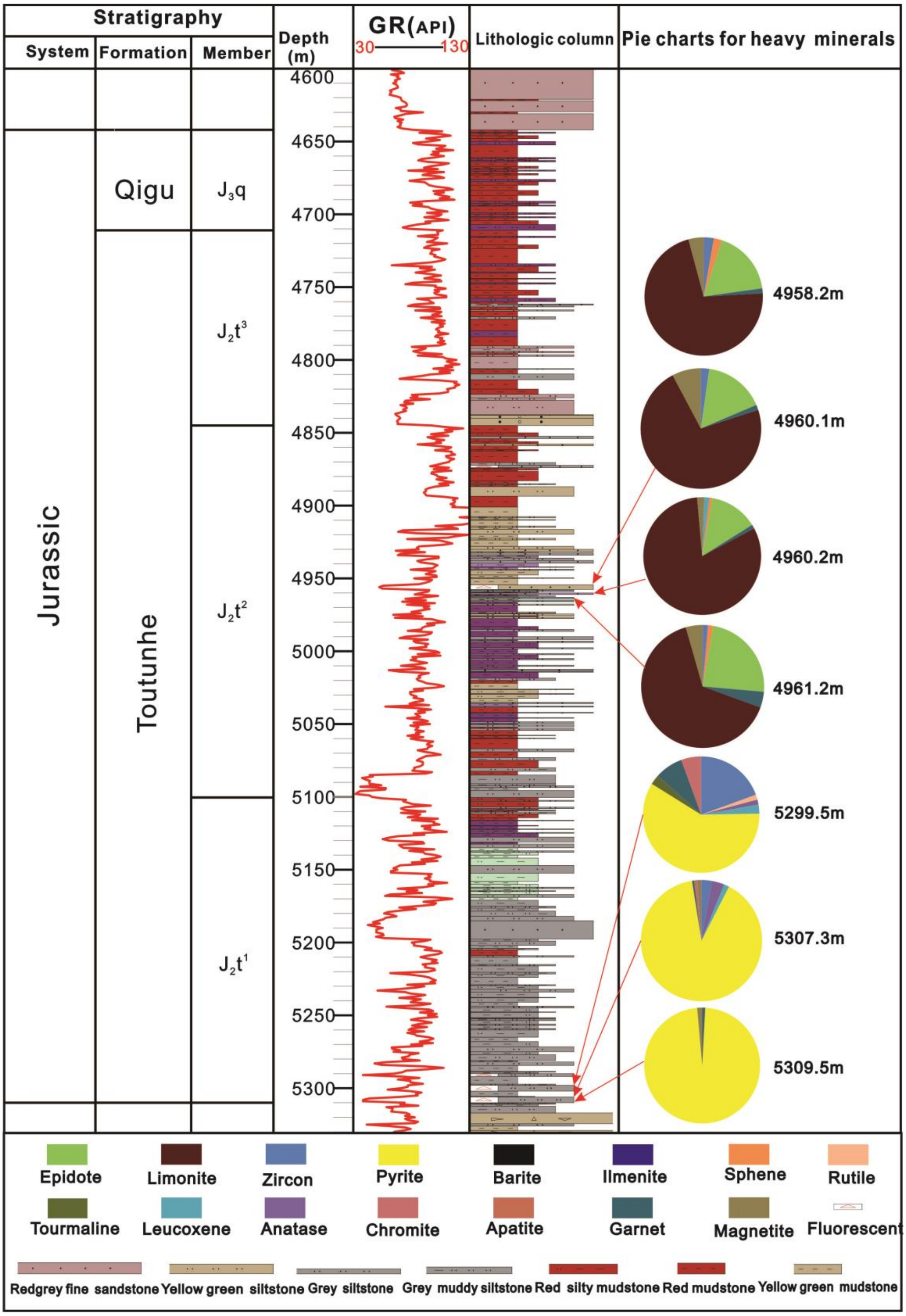

948

949 Fig. 4 Percentage distribution of heavy minerals in the Shishugou Group sandstones

950 of well D1

951

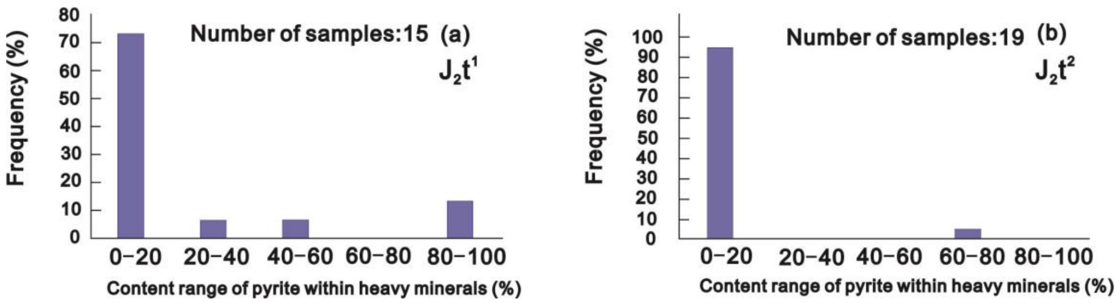

Fig. 5 The relative content of pyrite in the heavy mineral component of different strata. a: content range of pyrite in heavy minerals in J_2t^1. b: content range of pyrite in heavy minerals in J_2t^2.

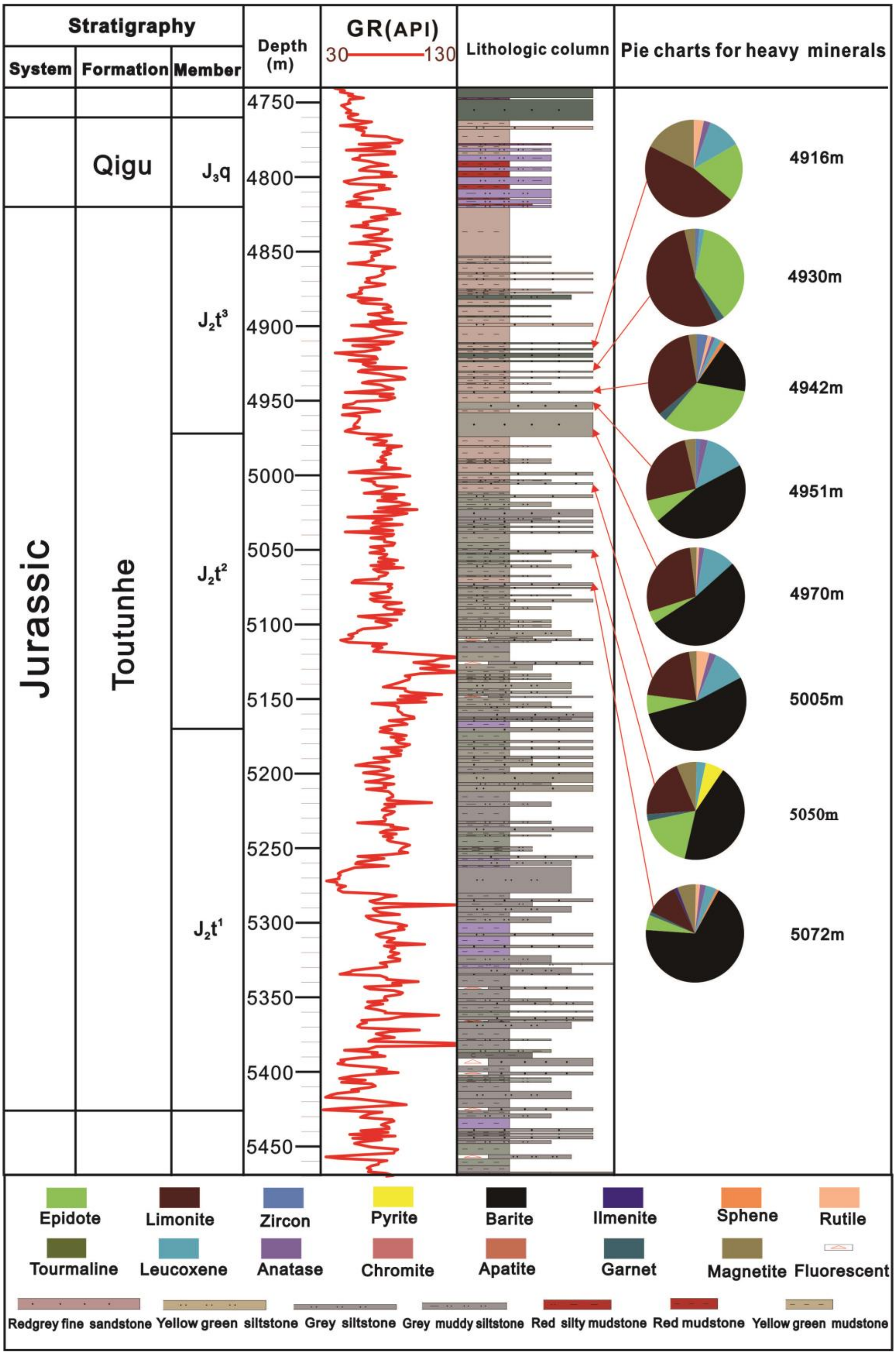

Fig. 6 Percentage distribution of heavy minerals in the Shishugou Group sandstones of well D101

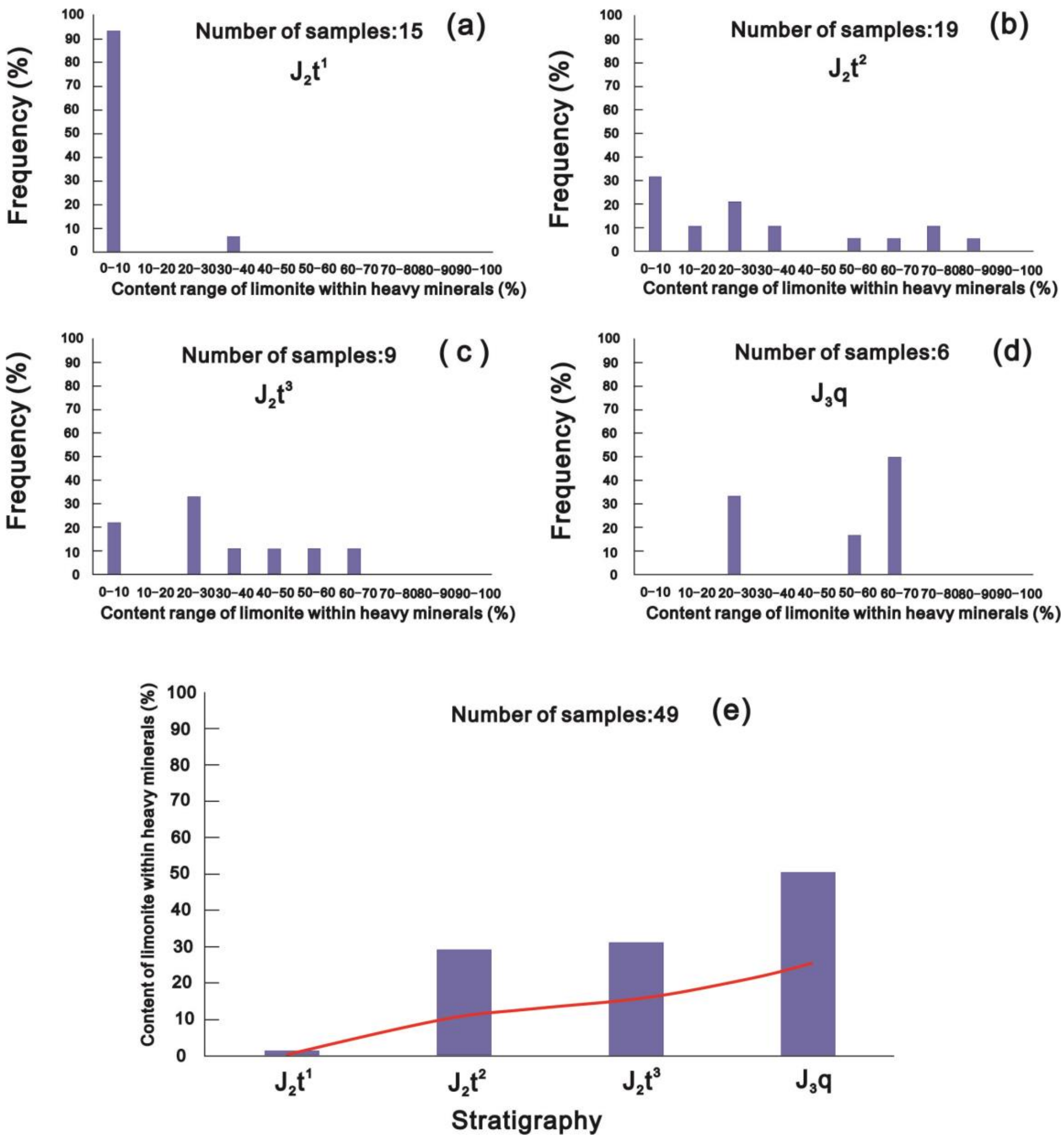

Fig. 7 Limonite content of heavy minerals in different strata. A: content range of limonite within heavy minerals in the J_2t^1 stratum. B: content range of limonite within heavy minerals in the J_2t^2 stratum. C: content range of limonite within heavy minerals in the J_2t^3 stratum. D: content range of limonite within heavy minerals in the J_3q stratum. E: content change of limonite within heavy minerals in different strata.

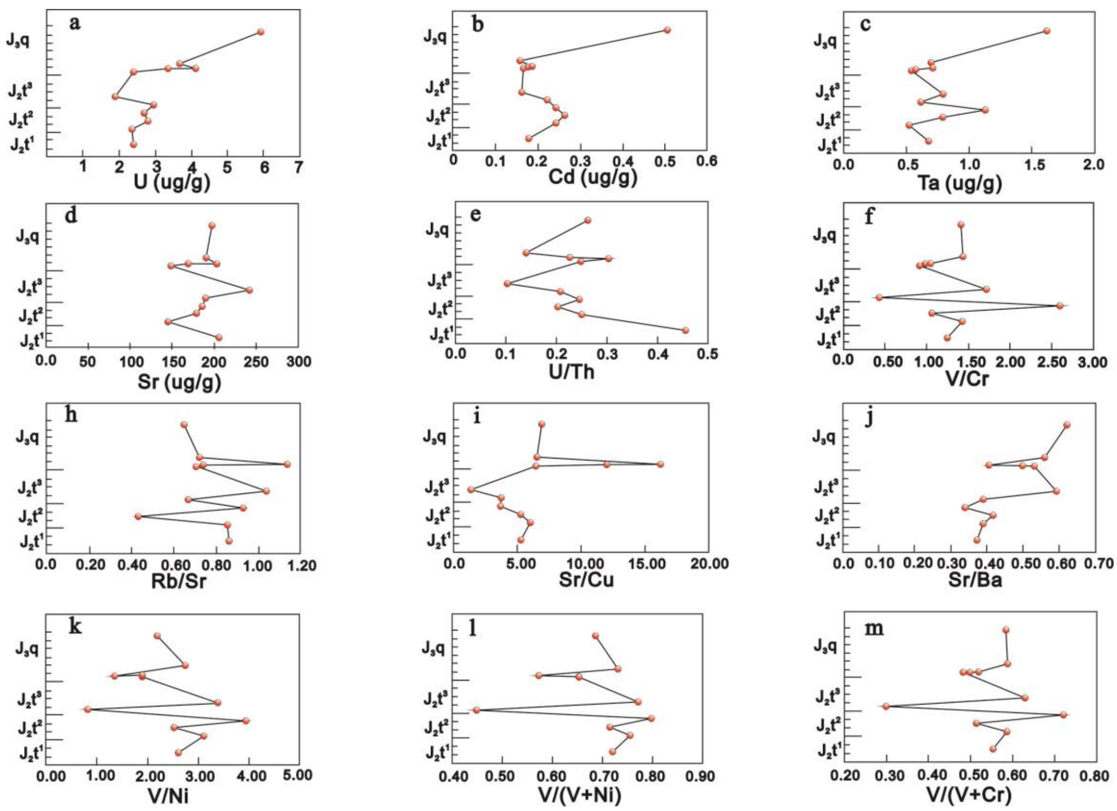

Fig. 8 Vertical change of trace elements and ratios in the Shishugou Group mudstone

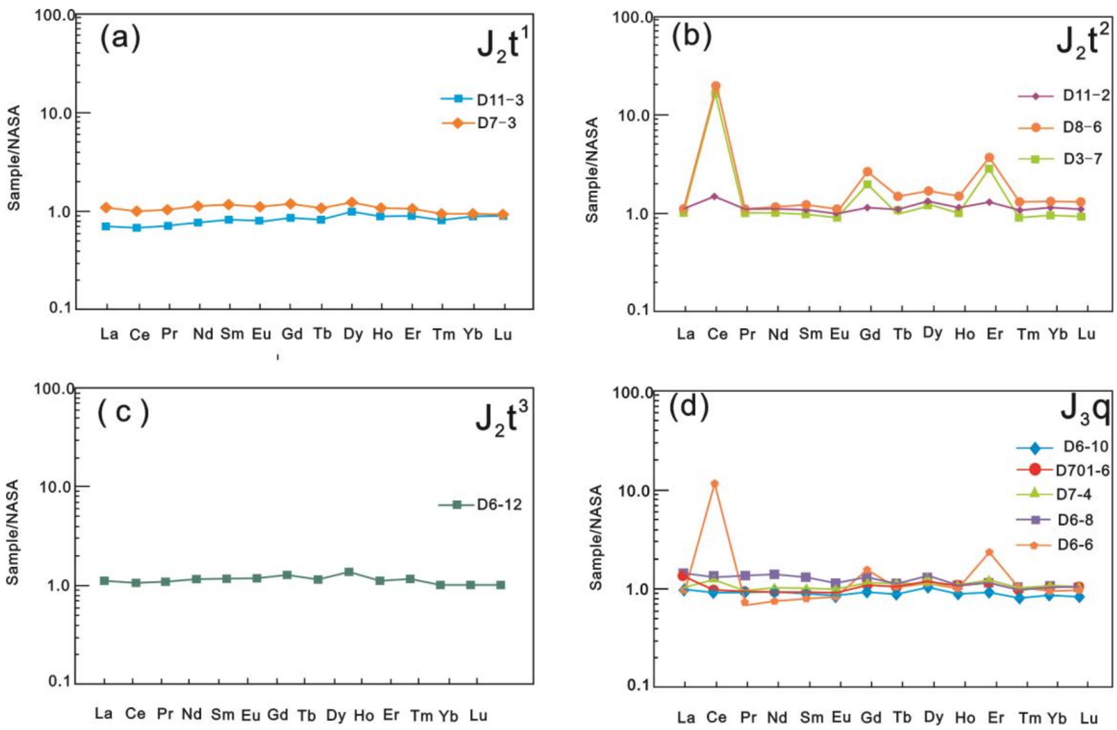

Fig. 9 NASA -normalised rare earth element (REE) patterns for the mudstone samples from J_2t^1 (a), J_2t^2 (b), J_2t^3 (c) and J_3q (d).

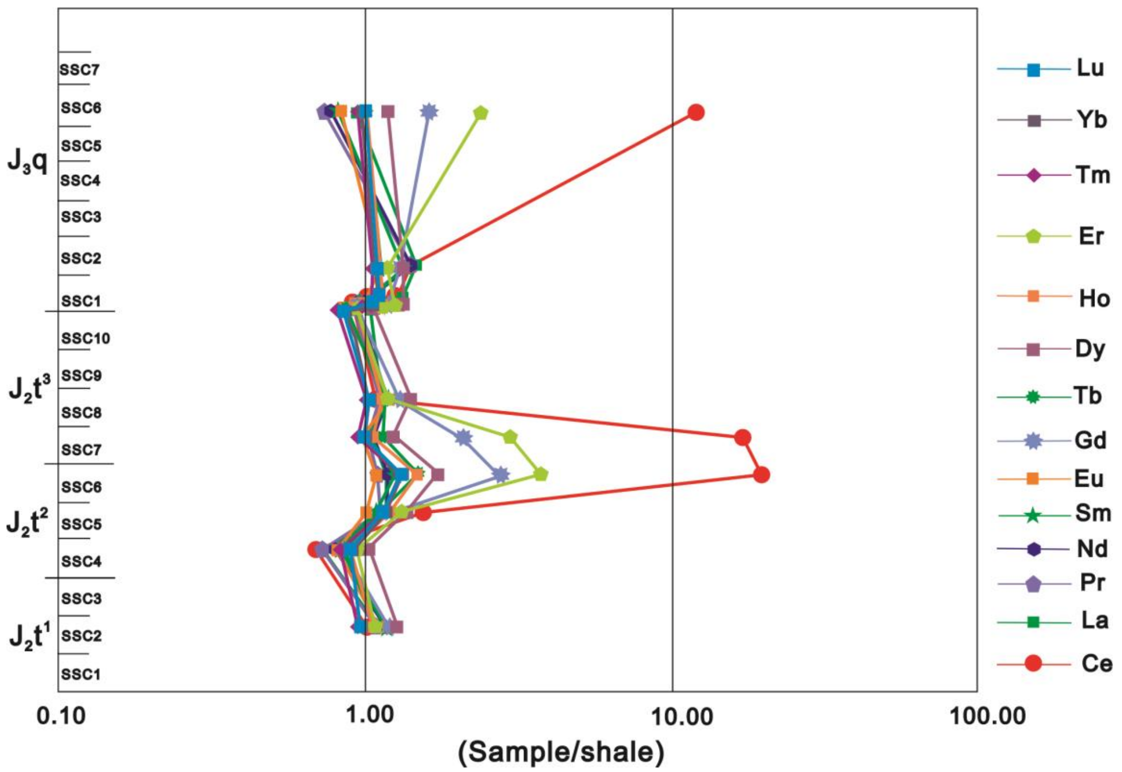

988
989 Fig. 10 Vertical change of shale-normalised (NASA) rare earth element (REE) in the
990 Shishugou Group mudstone
991

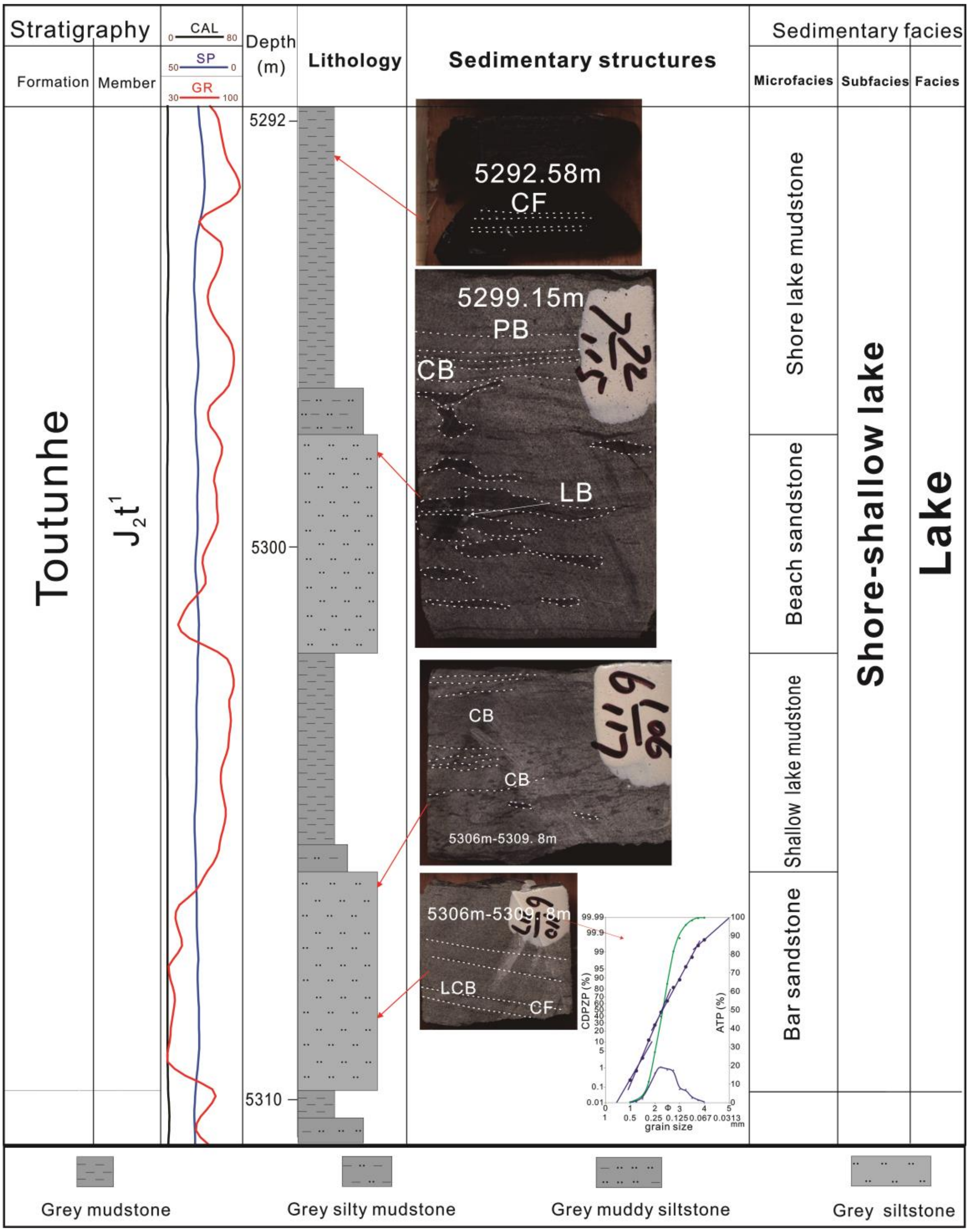

Fig. 11 Lithofacies, logging characteristics, sedimentary structures and sedimentary facies analysis of facies association A.CF= Carbon fragment; PB=Parallel bedding; CB= Current bedding; Lenticular bedding; LCB=Low-angle cross bedding; CDPZP=Cumulative distribution of particle size probability; ATP=Arithmetic percentage.

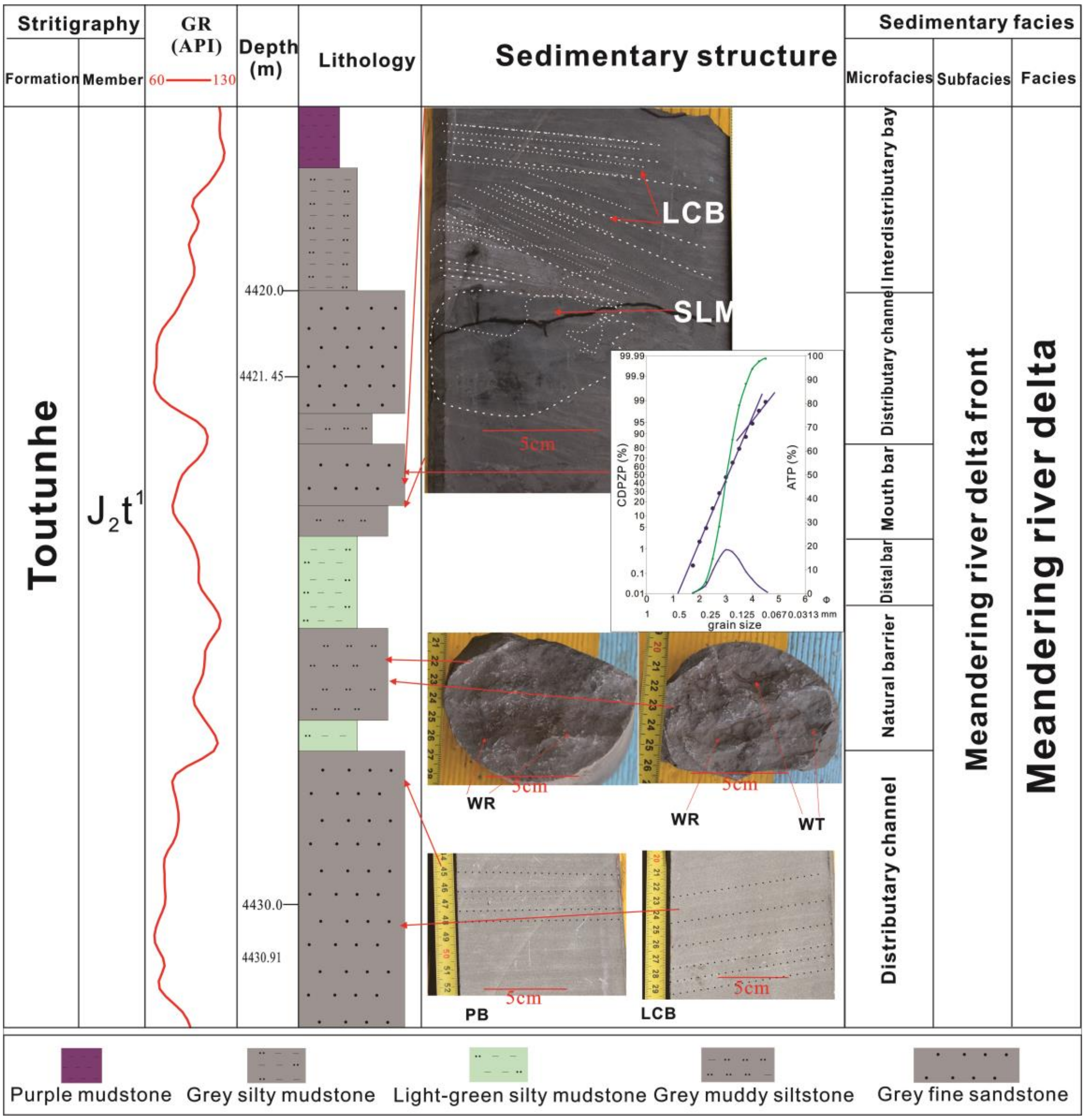

Fig. 12 Lithofacies, logging characteristics, sedimentary structures and sedimentary facies analysis of facies association B. CF= Carbon fragment; PB=Parallel bedding; CB= Current bedding; Lenticular bedding; LCB=Low-angle cross bedding; WR=Wave ripples; WT=Wormtrail; CDPZP=Cumulative distribution of particle size probability; ATP=Arithmetic percentage.

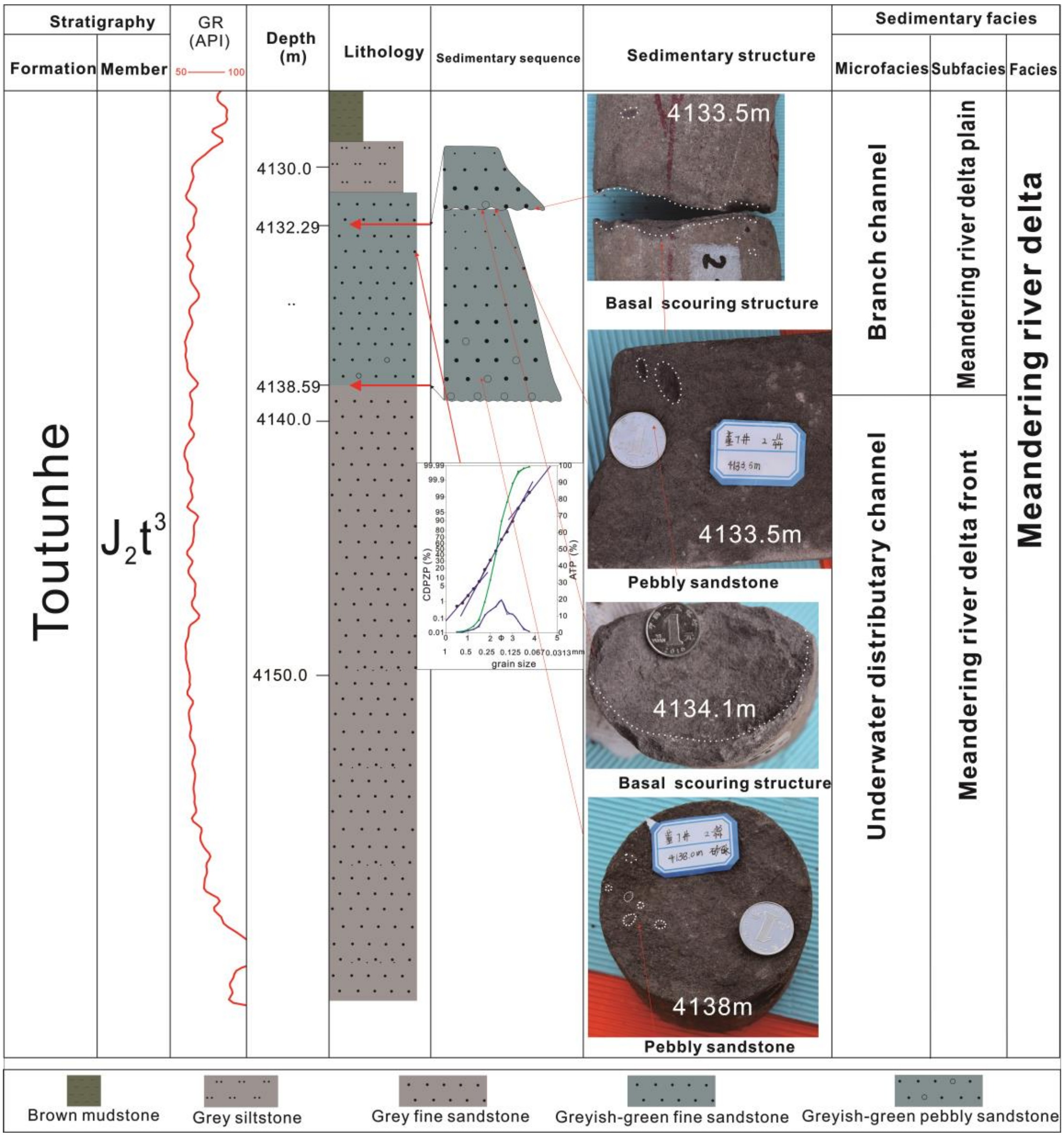

Fig. 13 Lithofacies, logging characteristics, sedimentary structures and sedimentary facies analysis of facies association C. CDPZB=Cumulative distribution of particle size probability; ATP=Arithmetic percentage.

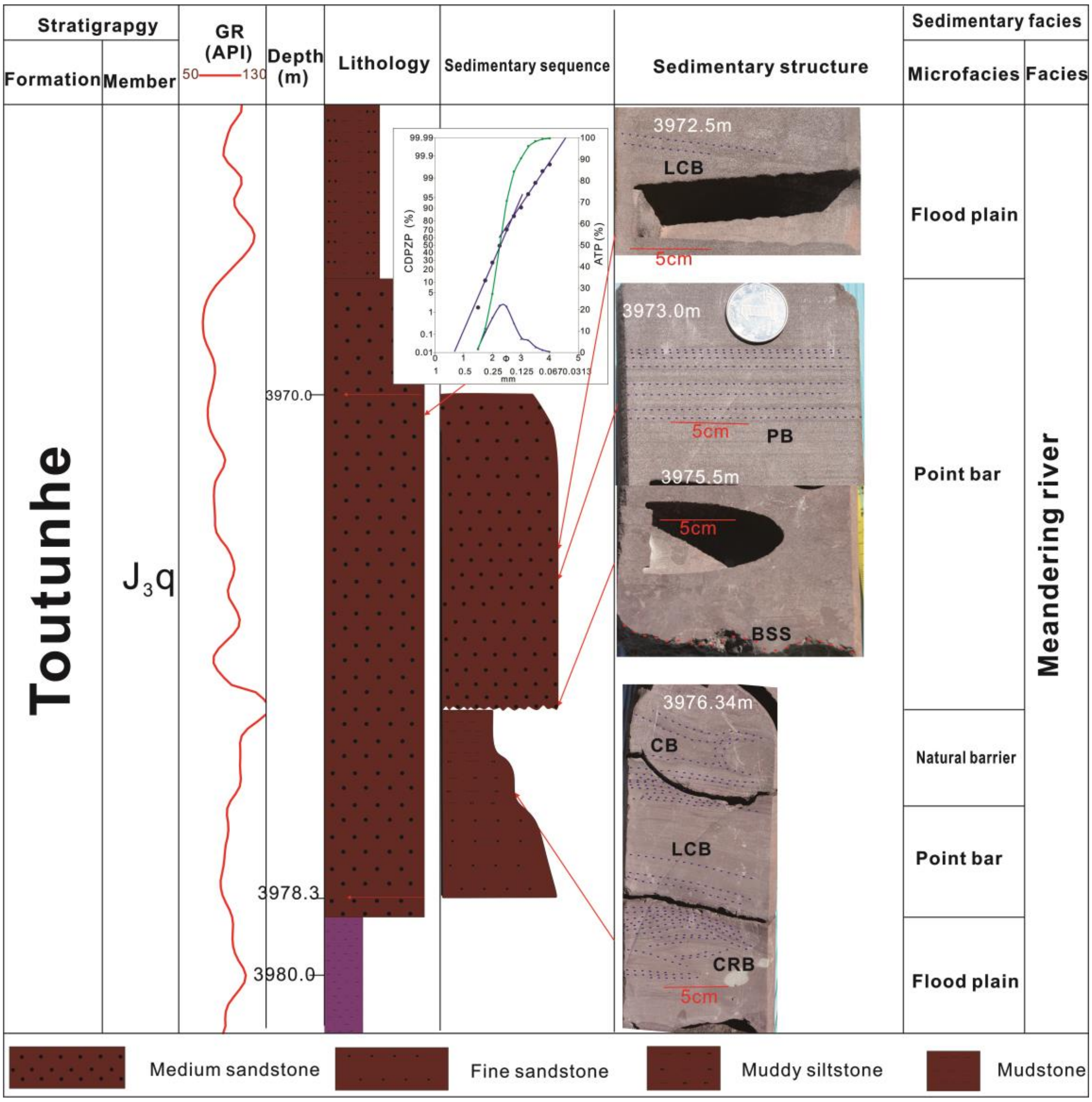

Fig. 14 Lithofacies, logging characteristics, sedimentary structures and sedimentary facies analysis of facies association D. CF= Carbon fragment; PB=Parallel bedding; CB= Current bedding; Lenticular bedding; LCB=Low-angle cross bedding;CRB=Climbing ripple bedding; BSS=Basal scouring structure; CDPZB=Cumulative distribution of particle size probability; ATP=Arithmetic percentage.

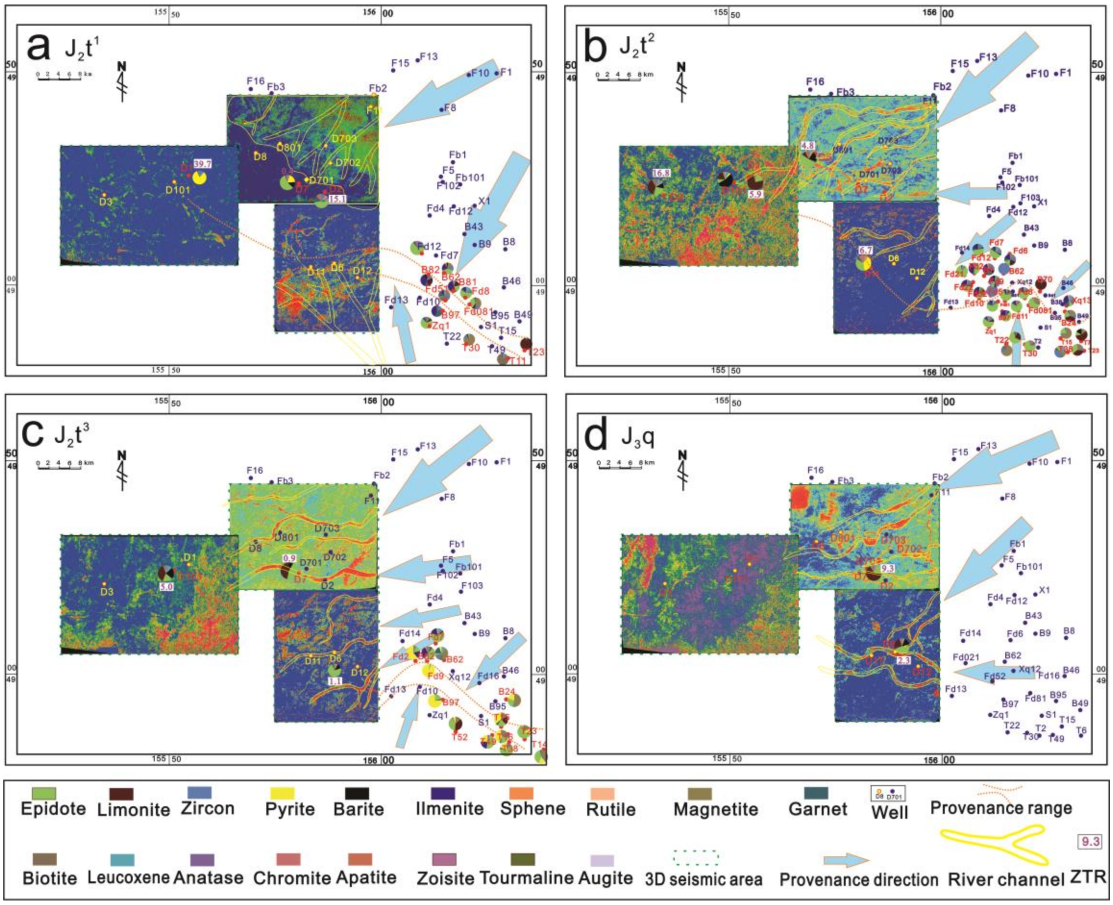

Fig. 15 The heavy mineral distribution, 3D-seismic slices (amplitude attribute), and the analysis of provenance and sedimentary system in the J_2t^1 (A), J_2t^2 (B), J_2t^3 (C) and J_3q (D) (The heavy minerals data in East Fukang slope from Ji et al.,2014). A : 3D-seismic slices showing many channels along northeastern trend and some south sediment source, the distribution (the relative contents of epidote in northeastern and in south Zq1well are higher than the middle) and ZTR (ZTR value increase toward southwest) of heavy minerals northeastern and south provenance; B: 3D-seismic slices showing channels along northeastern and eastern trend, the distribution (the relative contents of epidote decrease toward southwesten in most part of study area and increase toward southern in southeastern part of study area) and ZTR (ZTR value increase toward southwest) of heavy minerals showing main northeastern and eastern provenances and

limited south provenance; C: 3D-seismic slices showing channels along northeastern and eastern trend, the distribution (the relative contents of epidote decrease toward southwesten in most part of study area and increase toward southern in southeastern part of study area) and ZTR (ZTR value increase toward southwest) of heavy minerals showing main northeastern and eastern provenances and limited south provenance; D: 3D-seismic slices showing channels along northeastern trend and east-west trend, the distribution (the relative contents of epidote decrease toward east-west trend) and ZTR (ZTR value increase toward east-west trend) of heavy minerals showing northeastern and eastern provenances;

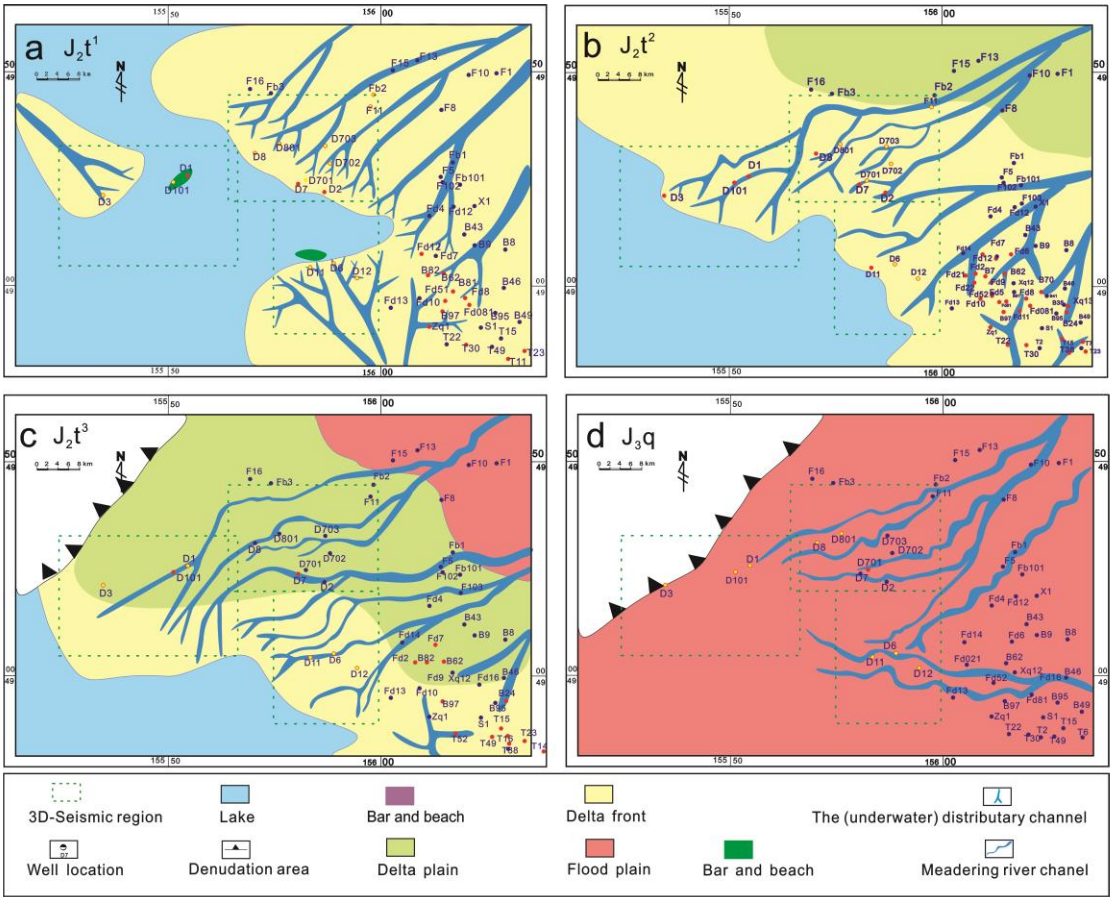

Fig. 16 Distribution characteristics of sedimentary facies in different formations of Shishigou Group in the Centeral-eastern Fukang Sag. A=The sedimentary facies of first member of Toutunhe Formation(J2t1); B= The sedimentary facies of second member of Toutunhe Formation(J2t2); C= The sedimentary facies of third member of Toutunhe Formation(J2t3); The sedimentary facies of Qigu Formation(J3q);

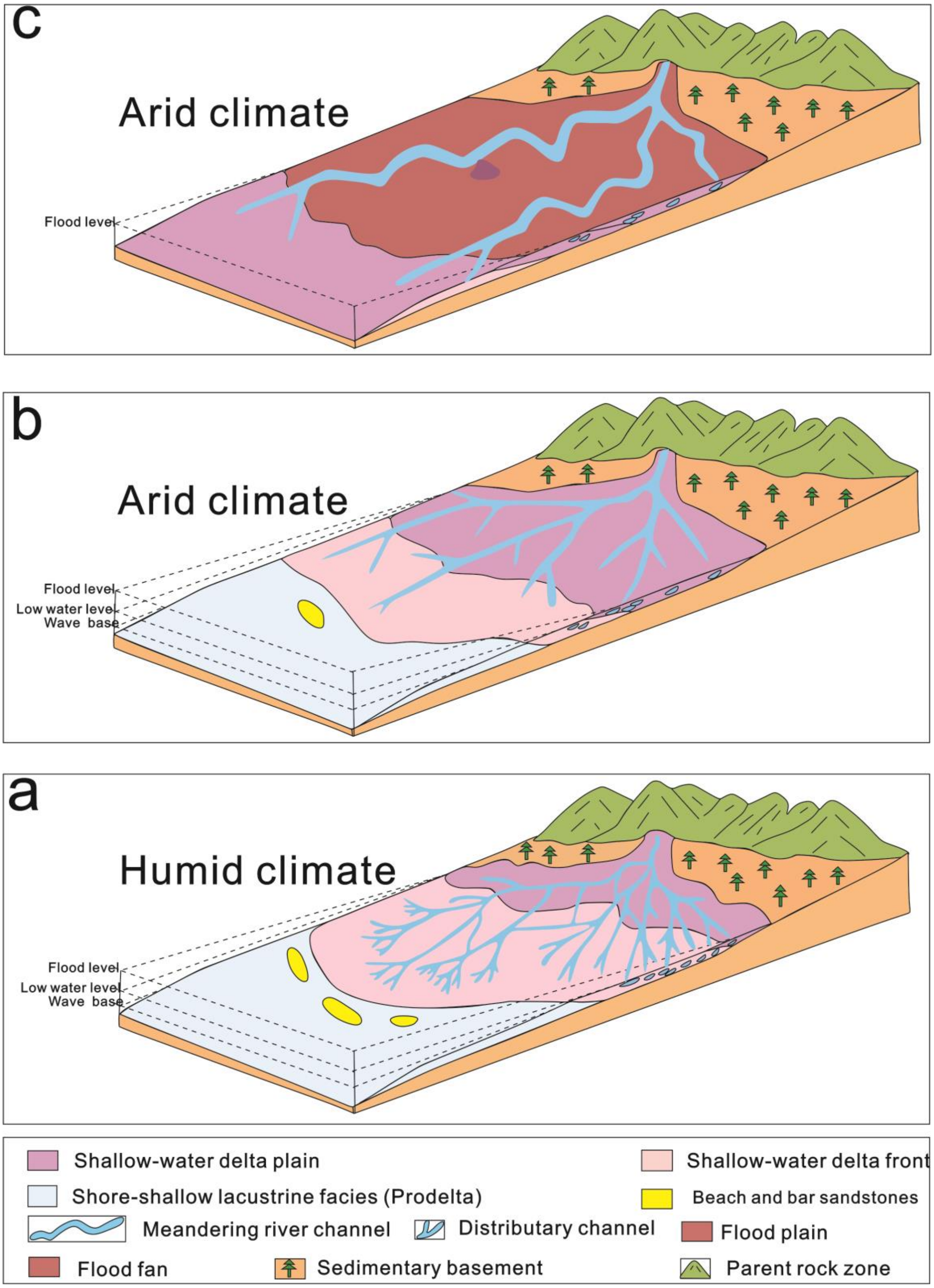

Fig. 17 Sedimentary model for the lake-shallow water delta-meandering river sedimentary system in different climate conditions. Modified from Zhu et al., 2012.

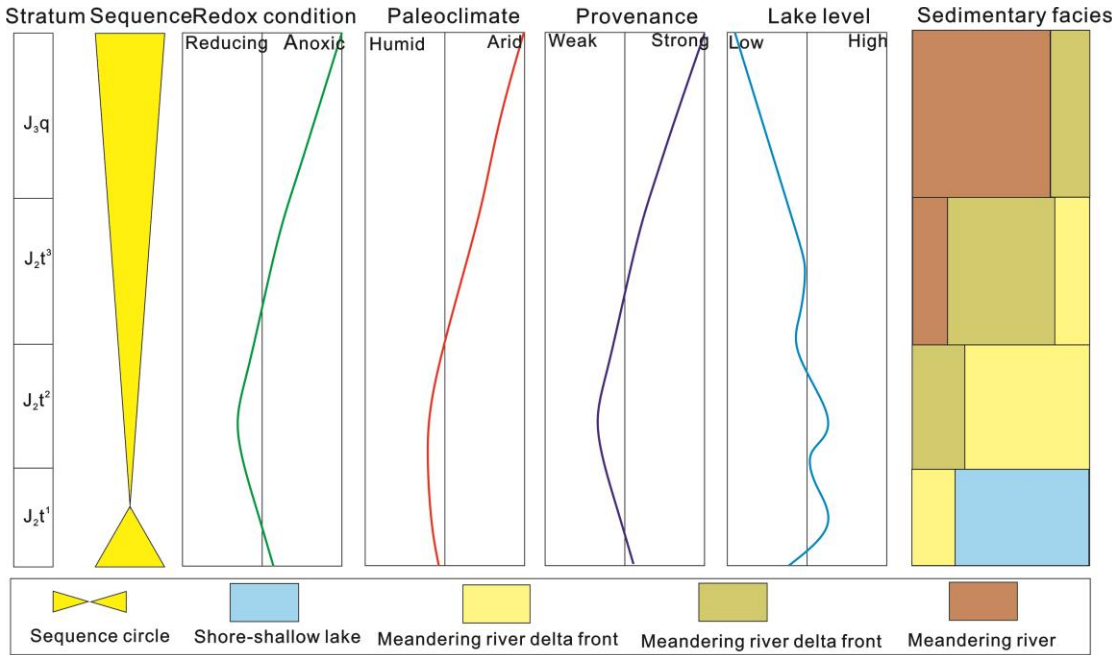

Fig. 18 The relationship between the palaeo-environment, provenance, lake level and sedimentary facies during deposition of the Middle-Late Jurassic Shishugou Group in the Central Juggar Basin. Lake level curve was modified from the Zhu et al. (2017).